Theory of intense-field dynamic alignment and high-order harmonic generation from coherently rotating molecules and interpretation of intense-field ultrafast pump-probe experiments

A. Abdurrouf[1,2,*] and F. H. M. Faisal[1,†]
[1]*Fakultät für Physik, Universität Bielefeld, Postfach 100131, D-33501 Bielefeld, Germany*
[2]*Department of Physics, University of Brawijaya, Malang 65145, Indonesia*
(Received 7 October 2008; published 4 February 2009)

A quantum theory of intense-field pump-probe experiments proposed by us recently [F. H. M. Faisal *et al.*, Phys. Rev. Lett. **98**, 143001 (2007) and F. H. M. Faisal and A. Abdurrouf, Phys. Rev. Lett. **100**, 123005 (2008)] is derived here fully and applied to investigate the phenomena of dynamic alignment and high-order harmonic generation (HHG) from coherently rotating linear molecules. The theory is developed from the basic quantum transition amplitude for the HHG and used to relate the Fourier transform (FT) of the expectation value of the dipole operator to the *rate* of emission of the HHG photons. It permits us to give analytical expressions for the HHG signals and their simultaneous dependence on the two externally available control parameters—the delay-time, t_d, between the pump and the probe pulse, and the relative angle, α, between their polarizations. A relation between the basic "one-molecule" and the macroscopic "many-molecule" HHG signals is obtained from the phase-matching condition for HHG in an ideal medium. The requirement for the coherent HHG signal and the "elastic" molecular transition, in contrast to the "inelastic" transitions and the "hyper-Raman" emission, is discussed. The effect of the "delayed" probe pulse on the dynamic alignment induced by the pump-pulse, the mean rotational energy of the molecule during the period between the pump and the probe pulse, as well as a method of estimating the effective temperature of the molecules are analyzed. A "revival theorem" on the number of fractional "revivals," equal to the lowest power of the "cosine operator" in the Hamiltonian of the system, times the maximum powers of the "cosine-moments" present in the signal, is derived and used to interpret the observed fractional revivals and their relative *phases*. A "magic" polarization angle $\alpha_c = \arctan\sqrt{2} \approx 55°$, at which the signals for all t_d approach each other closely, is identified as a generic signature of a σ_g symmetry of the active orbital. Similarly, the presence of a "crossing neighborhood" near α_c is shown to be a generic signature of an active π_g orbital. At an operational angle $\alpha_c \approx 55°$ in the laboratory, a *steady* emission of high-order harmonic radiation from coherently rotating molecules with σ_g orbital symmetry (e.g., N_2) can be obtained. Finally, explicit numerical calculations are performed at specific experimental parameter values in the time domain as well as in the frequency domain. The results well reproduce all the salient features of the experimental observations for N_2 and O_2, and provide a unified theoretical interpretation of the same.

DOI: 10.1103/PhysRevA.79.023405 PACS number(s): 32.80.Rm, 32.80.Fb, 34.50.Rk, 42.50.Hz

I. INTRODUCTION

In recent years, there has been much interest and progress in understanding the interaction of atoms and molecules with intense laser fields (e.g., [1,2]). Among the phenomena observed, high-order harmonic generation (HHG) is of particular interest, no less because of its potential applications as a source of coherent ultraviolet light and/or for generation of ultrashort attosecond laser pulses. In contrast to atoms, molecules have extra degrees of freedom such as vibration and rotation of the molecular frame, and have additional symmetry properties that give rise to richer physical phenomena when they interact with intense laser pulses. Among them is the phenomenon of alignment of linear molecules by strong and long laser pulses, which has been investigated in the past [3–6]. Much interest has recently been generated by the observation of recurrent dynamic alignments of linear molecules such as N_2 and O_2 [7,8] interacting with intense ultrashort laser pulses. They are monitored, for example, by nondestructive high-order harmonic generation signals from pump-probe experiments with delayed pairs of intense ultrashort pulses [9–13]. The dynamic HHG signals have led to suggestions of a "tomographic reconstruction" of the active molecular orbital [14–16], and to investigations of proton motions [17] or molecular dynamics [18].

In this paper, we derive fully a recently proposed [19,20] quantum theory of intense-field dynamic alignment and high-order harmonic generation from linear molecules, and we apply it to analyze the observed dynamical HHG signals for N_2 and O_2 molecules. Theoretical expressions for the signals are given analytically as a simultaneous function of the two external operational parameters—the delay time t_d and the relative polarization angle α between the pump and the probe pulse [9–13].

Before proceeding further, we briefly discuss the main experimental characteristics of dynamic alignment and the HHG signals as observed for N_2 and O_2. We recall at the outset that the quantum measure of dynamical alignment of a rotating molecule is the expectation value of the "alignment operator" $\cos^2\theta$: $A(t_d) \equiv \langle\langle \cos^2\theta \rangle\rangle(t_d)$, where θ is the angle between the molecular axis and the pump polarization direction; the double angular brackets stand for the expectation

*a.abdurrouf@googlemail.com
†ffaisal@physik.uni-bielefeld.de

value with respect to the wave-packet states (inner brackets) and the statistical average with respect to the Boltzmann distribution (outer brackets) of the initially occupied rotational states. It was observed experimentally [9–13] that the dynamic (or delay-time-dependent) HHG signal for N_2 mimicked the "alignment measure" $A(t_d)$. It exhibited the phenomenon of rotational revivals [3,6,21] including the "full-revival" with a period $T_r=\frac{1}{2Bc}$, where B is the rotational constant [22], as well as a $\frac{1}{2}$-revival and a $\frac{1}{4}$-revival. They are consistent with the time dependence of $A(t_d)$ defined above, since the operator $\cos^2\theta$ can couple the rotational states with $\Delta J=\pm 2$ (Raman allowed transitions) within the rotational states of the induced wave packets, and thus can give rise to the fractional revival periods associated with the corresponding beat frequencies. In the case of O_2, unexpectedly, an additional $\frac{1}{8}$-revival appeared in the HHG signal [11–13]. The latter is impossible for the alignment measure $A(t_d)$ to account for, since it cannot couple the rotational states with $\Delta J=\pm 4$, which is necessary to give rise to a beat period $\frac{1}{8}T_r$. Thus, to fit their data of O_2, Itatani *et al.* [11] proposed, empirically, to consider the expectation value of the operator $B(t_d)\equiv\langle\langle\sin^2 2\theta\rangle\rangle(t_d)$. Subsequently, some of the early theoretical models of the HHG signal (e.g., [23–25]) gave a similar result for O_2 and thus appeared to justify the empirical fit. Such a model also suggested that the maximum HHG signal for N_2 can occur when the field polarization and the molecular axis were parallel, whereas the maximum signal of O_2 would occur when they are "diagonal" (i.e., make an angle $\theta=45°$). However, these models could not consistently account for other effects that are discussed below. Unlike the time-dependent signals, their Fourier transforms (FT), which give rise to sharply defined individual spectral lines and series, can provide an alternative (and more precise) means of studying the dynamic alignment phenomenon. More recent experimental observations of the dynamic HHG signals for N_2 and O_2 and their FT have revealed surprising characteristics that cannot be fully understood in terms of the earlier considerations. Thus, we mention the following:

(a) Kanai *et al.* [12] found that their experimental HHG signals for N_2 and O_2 could not be well fitted, respectively, by the expectation values of the operators $\cos^2\theta$ and $\sin^2 2\theta$ alone. Thus, they were led to consider empirically additional operators involving *higher* powers of $\cos^2\theta$, or Legendre polynomials, for data-fitting purposes.

(b) Miyazaki *et al.* [13] measured the dynamical HHG signals of N_2 and O_2 and Fourier transformed their signals and found not only spectral series containing strong Raman allowed but also weak Raman forbidden and anomalous lines, for both N_2 and O_2.

(c) Itatani *et al.* [14] observed that the HHG signal from dynamically aligned N_2 was enhanced when the pump polarization was taken parallel to the probe polarization, and was suppressed when the polarizations were taken to be perpendicular.

(d) Kanai *et al.* [12] and Miyazaki *et al.* [13,26] measured the HHG signal for the diatomic N_2, O_2, and the triatomic CO_2, for different relative angles α between the pump and probe polarizations, and they observed that the HHG signal modulations are not only smaller in the perpendicular case, compared to the parallel case, but also are of *opposite phase* in the two geometries.

(e) Kanai *et al.* [12] proposed a planar emission model of HHG, which produced an opposite phase relation, as observed, but it did not yield the *unequal* modulation amplitudes observed in the two geometries.

(f) The present theory predicted (cf. [20] and below) a "magic" polarization angle, $\alpha_c\approx 55°$, at which the harmonic emission from coherently rotating molecules with σ_g orbital symmetry (e.g., N_2) becomes equal for *all* delay times t_d. Most recent observations by Yoshii *et al.* [27] appear to confirm the same.

In this paper, we present an *ab initio* development of the above-mentioned theory [19,20] that is shown to provide a unified theoretical account of all the phenomena noted above and other related characteristics of dynamic alignments and HHG signals, as well as their Fourier spectra. We begin with a short schematic description of a typical intense-field pump-probe experiment on dynamic alignments and the molecular HHG signals. They are investigated as a function of (a) the time delay t_d and (b) the relative polarization angle α between the pump and probe pulse. In Secs. II–IV, we systematically derive the S-matrix theory of molecular alignment and dynamic HHG signal from an ensemble of freely rotating linear molecules, discuss the connection between the "one"- and the "many"-molecule signals, and derive the relation between the quantum amplitude for the emission of a HHG photon and the expectation value of the transition dipole moment. In Sec. V, we apply the theory to N_2 and O_2 molecules and give the analytic formulas for the "HHG operators" and the HHG *signals* that are valid for any polarization angles, α, and any delay times, t_d. In Sec. VI, we use the formulas for N_2 and O_2 to calculate the HHG signals for specific experimental parameters, both in the time and frequency domain, and we discuss the results with reference to the experimental observations. In Sec. VII, we investigate a number of problems of general interest, including the influence of the probe pulse on the dynamic alignment, the effect of the initial temperature on the HHG signal, and the *mean energy* of the rotating molecule after interaction with the pump pulse. Next, we consider two other definitions used earlier for the HHG signal and point out their differences with respect to the present theory and observations. Finally, we investigate the case of "adiabatic alignment" of linear molecules simply by using the present theory in the limit of a long pulse duration. We conclude with a summary in Sec. VIII.

In Fig. 1, we show a schematic of a typical intense-field pump-probe experiment. A laser beam is first split into two parts, L_1 and L_2, by a beam splitter (BS) with a desired ratio of the beam intensities. The probe-pulse L_2 is delayed by passing through a delay line system (D), by a finite amount t_d, with respect to the pump-pulse L_1, and both are sent through a beam mixer (BM), coparallel, to the target gas molecules from a gas jet. The high-order harmonic signal produced by the probe pulse is recorded by the detector system for each selected value of t_d. In addition, a polarizer P can be inserted to rotate the angle of polarization of the probe pulse with respect to the polarization direction of the pump pulse at any desired angle α. The pulses are generally

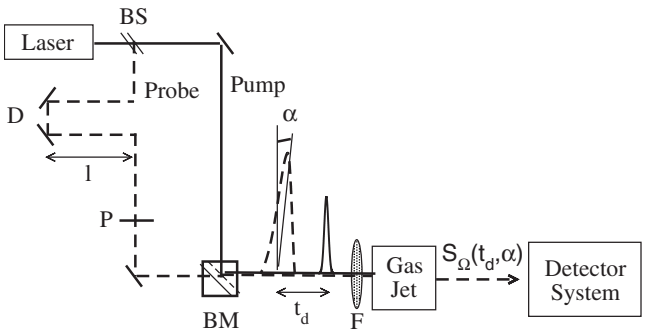

FIG. 1. A scheme of a typical pump-probe experiment. See text for further explanation.

assumed to be effectively nonoverlapping ($t_d \neq 0$) and they are shorter than the period of the rotational degrees of freedom of interest. Note that both t_d and α provide controllable parameters on the high-order harmonic emission process from the outside.

II. A QUANTUM THEORY OF INTENSE-FIELD PUMP-PROBE EXPERIMENTS AND MOLECULAR HIGH-ORDER HARMONIC GENERATION SIGNALS

A. Total Hamiltonian and equations of motions of the dynamical system

Within the adiabatic Born-Oppenheimer approximation of the target molecule, the total Hamiltonian of the system can be written [19] (in a.u.: $e=\hbar=m=\alpha c=1$) as

$$H_{\text{tot}}(t) = H_N + V_{N\text{-}L_1}(t) + H_e + V_{e\text{-}L_2}(t-t_d), \tag{1}$$

where H_N is the nuclear Hamiltonian, $V_{N\text{-}L_1}(t)$ is the interaction due to the pump pulse with the nuclear motion at a time t, H_e is the electronic Hamiltonian, and $V_{e\text{-}L_2}(t-t_d)$ is the interaction of the probe pulse with the active electron at a delay t_d. We describe the two laser pulses (in the long-wavelength dipole-approximation) $F(\phi_j(t)) \equiv f(t)\cos[\phi_j(t)]$ and the corresponding vector potentials by $A(\phi_j(t)) = -\frac{c}{\omega} f(t)\sin[\phi_j(t)]$, where $f(t)$ is the envelope of the electric field [28].

The phase $\phi_j(t)$ of the field at the position of the active electron of the molecule is given by $\phi_j(t) = (\omega t - \mathbf{k}_\omega \cdot \mathbf{X}_j)$, where the center of mass (C.M.) of the molecule is assumed to be located at a position "$\mathbf{X}_j$"; ω and $\mathbf{k}_\omega$ are the laser of frequency and the wave number, respectively. For the sake of simplicity of writing, we may suppress the $\mathbf{X}_j$ and/or the index j and t dependence of the phase factor $\phi_j(t)$, unless otherwise needed explicitly. It will be shown below that the coherent signal appears for the "elastic" scattering (the final state of the molecule is the same as the initial state), and (for an ideal gas medium) along the forward direction of the incident field (cf. [[2] Sec. 4], and references cited in that section).

Thus, we write the laser-molecule interaction Hamiltonians appearing above as

$$V_{N\text{-}L_1}(t) = -\mu F_1(t) - \frac{1}{2}\sum_{ij} F_{1i}(\phi(t))\alpha_{ij}F_{1j}(\phi(t)), \tag{2}$$

where μ is the permanent dipole moment (if nonzero) and α with Cartesian components α_{ij}; $(i,j)=(1,2,3)$ is the polarizability *tensor* of the molecule (always nonzero); and

$$V_{e\text{-}L_2}(t-t_d) = -\hat{\boldsymbol{d}}_e \cdot \boldsymbol{F}[\phi(t-t_d)], \tag{3}$$

where $\hat{\boldsymbol{d}}_e$ stands for the electronic dipole *operator*.

B. Total wave function in intense-field *S*-matrix theory

We first consider a systematic solution of the time-dependent Schrödinger equation of the system

$$i\frac{\partial}{\partial t}\Psi(t) = H_{\text{tot}}(t)\Psi(t) \tag{4}$$

using the general technique of intense-field many-body *S*-matrix theory (IMST) [2]. In this approach, the total wave function of the system satisfying a given initial (final) condition can be written as a series expansion in such a way that the dominant virtual states, when present, can appear already in the leading terms of the series. To this end, we introduce three partitions of the same total Hamiltonian "reference" Hamiltonians and the corresponding interactions in the initial, "i," final, "f," and intermediate (virtual) states, "0,"

$$H_{\text{tot}}(t) = H_i + V_i(t) = H_f(t) + V_f(t) = H_0(t) + V_0(t). \tag{5}$$

It is also useful to define the reference Green's functions associated with the reference Hamiltonians, $H_s(t)$; $s \equiv i,f,0$,

$$\left(i\frac{\partial}{\partial t} - H_s(t)\right)G_s(t,t') = \delta(t-t'). \tag{6}$$

In general, the Green functions can be obtained from the complete set of the fundamental solutions, $|\psi_j^{(s)}(t)\rangle$, of the Schrödinger equations governed by the reference Hamiltonians $H_s(t)$; $s=i,f,0$,

$$G_s(t,t') = -i\theta(t-t')\sum_{all\ j} |\psi_j^{(s)}(t)\rangle\langle\psi_j^{(s)}(t')|. \tag{7}$$

The validity of the solutions Eq. (6) can be readily established by operating on the left-hand side of Eq. (7) with $[i\frac{\partial}{\partial t} - H_s(t))$, and using Eq. (6), the completeness of the fundamental solutions, $\Sigma_j |\psi_j^{(s)}(t)\rangle\langle\psi_j^{(s)}(t)| = \mathbf{1}$ and the equation $\frac{\partial}{\partial t}\theta(t-t') = \delta(t-t')$, to obtain a δ-function integration on the right-hand side, followed by the obvious simplification. Thus, we can express the total wave function of the interacting system, evolving from an arbitrary initial state, $|\chi_i(t)\rangle$, as a series,

$$|\Psi(t)\rangle = \sum_{j=0}^{\infty} |\Psi_i^{(j)}(t)\rangle, \tag{8}$$

with

$$|\Psi_i^{(0)}(t)\rangle = |\chi_i(t)\rangle, \tag{9}$$

$$|\Psi_i^{(1)}(t)\rangle = \int_{t_i}^{t_f} dt_1 G_f^0(t,t_1) V_i(t_1) |\chi_i(t_1)\rangle, \tag{10}$$

$$|\Psi_i^{(2)}(t)\rangle = \int_{t_i}^{t_f} \int_{t_i}^{t_f} dt_2 dt_1 G_f^0(t,t_2) V_f(t_2) G_0(t_2,t_1) \times V_i(t_1) |\chi_i(t_1)\rangle \cdots , \tag{11}$$

and

$$|\Psi_i^{(n)}(t)\rangle = \int_{t_i}^{t_f} \cdots \int_{t_i}^{t_f} \int_{t_i}^{t_f} dt_n \cdots dt_2 dt_1 G_f^0(t,t_n) \times V_f(t_n) \cdots G_0(t_3,t_2) V_f(t_2) G_0(t_2,t_1) \times V_i(t_1) |\chi_i(t_1)\rangle. \tag{12}$$

III. MANY-MOLECULE VERSUS ONE-MOLECULE SIGNALS

A. Transition amplitudes for high-order harmonic generation

Emission of a harmonic photon of frequency $\Omega = n\omega$ and wave vector $\boldsymbol{K}_\Omega$, from its vacuum state $|0_\Omega\rangle$ (zero occupation number in Fock space), into a singly occupied number state, $|1_\Omega\rangle$, is fundamentally a quantum electrodynamical process, i.e., due to the interaction of the active electron with the vacuum field albeit in the presence of the intense external laser field. Its theoretical formulation, therefore, clearly requires one to consider at least the combined state of the system, consisting of the direct product of the ordinary space of the laser field (semiclassical) plus molecule and the occupation number space of the vacuum and the emitted photon (cf., e.g., [[2], Sec. 4.5]). Nevertheless, exactly the same result for the single-photon HHG emission amplitude can also be obtained using the ordinary quantum mechanics, simply by taking the quantum electrodynamically normalized interaction $V^*(t)$ for the emission of a photon into the initially unoccupied vacuum mode of frequency Ω and wave vector $\boldsymbol{K}_\Omega$ (cf. [[29,30], Lecture 2]),

$$V^*(t) = N_\Omega e^{i\Phi_j(t)} \boldsymbol{\epsilon}_\Omega \cdot \hat{\boldsymbol{d}}_e. \tag{13}$$

In the above, $N_\Omega \equiv \sqrt{\frac{2\pi\hbar\Omega}{L^3}}$, L^3 is the quantization volume, $\boldsymbol{\epsilon}_\Omega$ is the polarization vector of the emitted photon, and $\boldsymbol{d}_e$ is the usual electronic transition dipole operator; the phase $\Phi_j(t) = (\Omega t - \boldsymbol{k}_\omega \cdot \boldsymbol{X}_j)$. As usual in the present dipole approximation, we have neglected the retardation factor, $e^{-i\boldsymbol{K}_\Omega \cdot \boldsymbol{r}} \approx 1$; we may note explicitly that the exact position of the electron with respect to an arbitrary coordinate origin is given by $\boldsymbol{X}_j + \boldsymbol{r}$, where as before $\boldsymbol{X}_j$ is the C.M. of the jth molecule and $\boldsymbol{r}$ is the position of the electron with respect to the C.M. of the molecule.

The HHG amplitude for the emission of a harmonic frequency Ω from the jth molecule is given (cf. [[2], Sec. 4]) by the sum of two "Feynman-like" diagrams, (a) and (b), shown in Fig. 2. The diagram (a) corresponds to the so-called "direct" amplitude (associated with the retarded Green's function), whereas the diagram (b) corresponds with the "time-reversed" amplitude (associated with the advanced Green's function). The amplitude for the harmonic emission process can be written down analytically from diagram (a) by reading in the forward (upward) direction of time: First, the molecule is prepared by the "pump" laser pulse in the state $i \equiv |\Phi_i(t)\rangle$. Next, the molecule interacts with the probe laser field (short horizontal line with a cross), then it propagates through $G_0 = G_0^{(+)}$ (vertical line). Next it interacts with the vacuum field by $V^{(*)}$ (horizontal line ending in Ω), and emits the harmonic photon of frequency Ω, and finally returns to the *same* state $i \equiv |\Phi_i(t)\rangle$ as before. A similar interpretation holds for the time reversed diagram (b) except that here the system evolves backward in time through $G_0 = G^{(-)}$. The quantum amplitude $A_j(\Omega)$, for the emission of the HHG photon of frequency Ω, and wave number $\boldsymbol{K}_\Omega$, from the molecule located at $\boldsymbol{X}_j$, is given by the *sum* of the two diagrams,

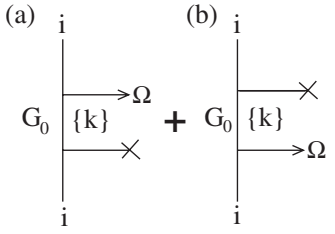

FIG. 2. Quantum amplitude for coherent emission of a high-order harmonic photon (frequency Ω) is the sum of a direct (a) and a time-reversed (b) diagram.

$$A_j(\Omega) = \text{diag}(a) + \text{diag}(b). \tag{14}$$

Mathematically, we have

$$\text{diag}(a) = -i \int_{-\infty}^{\infty} dt \int_{-\infty}^{\infty} dt' \langle \phi_i(t) | V^*(t) \times G_0^{(+)}(t,t') V_{e\text{-}L_2}(t' - t_d) | \chi_i(t') \rangle \tag{15}$$

and

$$\text{diag}(b) = -i \int_{-\infty}^{\infty} dt \int_{-\infty}^{\infty} dt' \langle \phi_i(t') | V_{e\text{-}L_2}(t' - t_d) \times G_0^{(-)}(t',t) V^*(t) | \chi_i(t) \rangle. \tag{16}$$

B. A relation between HHG amplitude and FT of the dipole expectation value

1. Recasting the quantum HHG amplitude

Before proceeding further, we consider the relation between the quantum HHG amplitude, Eq. (14), and the expectation value of the electric dipole operator, $\hat{\boldsymbol{d}}_e$, that is popularly used for calculations of HHG signals. To this end, we first rewrite the quantum amplitude Eq. (15) by introducing the first-order wave function $\Psi^{(1)}$ [cf. Eq. (10)] that arises from the initial state $|\chi_i(t)\rangle$ due to the interaction with the probe pulse,

$$|\Psi^{(1)}(t)\rangle = \int_{-\infty}^{\infty} dt' G_0^{(+)}(t,t') \times V_{e\text{-}L_2}(t'-t_d)|\chi_i(t')\rangle. \tag{17}$$

We may first rewrite Eq. (15) as

$$\begin{aligned}\mathrm{diag}(a) &= -i\int_{-\infty}^{\infty} dt\langle\chi_i(t)|V^*(t)|\Psi^{(1)}(t)\rangle \\ &= -i\int_{-\infty}^{\infty} dt e^{i(\Omega t - \boldsymbol{K}_\Omega\cdot\boldsymbol{X}_j)} \times \langle\chi_i(t)|N_\Omega \boldsymbol{\epsilon}_\Omega\cdot\hat{\boldsymbol{d}}_e|\Psi^{(1)}(t)\rangle,\end{aligned} \tag{18}$$

where we have used the explicit form of the interaction $V^*(t)$. Next we rewrite Eq. (16) using a standard relation satisfied by the advanced and the retarded Green functions (e.g., [30]),

$$G_0^{(-)}(t',t) = [G_0^{(+)}(t,t')]^*. \tag{19}$$

We also note that the laser-molecule interaction is real (Hermitian), i.e.,

$$V_{e\text{-}L_2}(t) = [V_{e\text{-}L_2}(t)]^*. \tag{20}$$

Thus, the integral over dt' in Eq. (16) can be rewritten as

$$\begin{aligned}\mathrm{diag}(b) &= -i\int_{-\infty}^{\infty} dt \int_{-\infty}^{\infty} dt' \langle\chi_i(t')|V_{e\text{-}L_2}(t'-t_d) \\ &\quad \times G_0^{(-)}(t',t)V^*(t)|\chi_i(t)\rangle \\ &= -i\int_{-\infty}^{\infty} dt \int_{-\infty}^{\infty} dt' \times [G_0^{(+)}(t,t')V_{e\text{-}L_2}(t'-t_d)|\chi_i(t')\rangle]^* \\ &\quad \times V^*(t)|\chi_i(t)\rangle \\ &= -i\int_{-\infty}^{\infty} dt\langle\Psi^{(1)}(t)|V^*(t)|\chi_i(t)\rangle \\ &= -i\int_{-\infty}^{\infty} dt e^{i(\Omega t - \boldsymbol{K}_\Omega\cdot\boldsymbol{X}_j)} \times \langle\Psi^{(1)}(t)|N_\Omega\boldsymbol{\epsilon}_\Omega\cdot\hat{\boldsymbol{d}}_e|\chi_i(t)\rangle.\end{aligned} \tag{21}$$

Hence, adding Eqs. (18) and (21), we get the quantum HHG amplitude in the suggestive form

$$\begin{aligned}A_j(\Omega) &= -iN_\Omega\boldsymbol{\epsilon}_\Omega\cdot\int_{-\infty}^{\infty} dt e^{i(\Omega t - \boldsymbol{K}_\Omega\cdot\boldsymbol{X}_j)} \times \{\langle\chi_i(t)|\hat{\boldsymbol{d}}_e|\Psi^{(1)}(t)\rangle \\ &\quad + \langle\Psi^{(1)}(t)|\hat{\boldsymbol{d}}_e|\chi_i(t)\rangle\} \\ &= -iN_\Omega\boldsymbol{\epsilon}_\Omega\cdot\int_{-\infty}^{\infty} dt e^{i(\Omega t - \boldsymbol{K}_\Omega\cdot\boldsymbol{X}_j)} \times \{\langle\chi_i(t)|\hat{\boldsymbol{d}}_e|\Psi^{(1)}(t)\rangle \\ &\quad + \mathrm{c.c.}\},\end{aligned} \tag{22}$$

where "c.c." stands for the complex conjugate.

2. Dipole expectation value

The expectation value of the dipole operator, $\boldsymbol{D}_{i,i}(t)$, can be calculated using the lowest-order KFR approximation [31–33] of the system wave function as follows:

$$\begin{aligned}\boldsymbol{D}_{i,i}(t) &= \langle\Psi(t)|\hat{\boldsymbol{d}}_e|\Psi(t)\rangle = \langle\chi_i(t)|\hat{\boldsymbol{d}}_e|\chi_i(t)\rangle + \{\langle\chi_i(t)|\hat{\boldsymbol{d}}_e|\Psi^{(1)}(t)\rangle \\ &\quad + \langle\Psi^{(1)}(t)|\hat{\boldsymbol{d}}_e|\chi_i(t)\rangle\} + \cdots \\ &= \{\langle\chi_i(t)|\hat{\boldsymbol{d}}_e|\Psi^{(1)}(t)\rangle + \mathrm{c.c.}\} + \cdots .\end{aligned} \tag{23}$$

Note that the zeroth-order term in the first line above vanishes for centrosymmetric systems; we have also neglected the quadratic powers of the first-order KFR correction (and the higher-order terms).

Combining Eq. (23) with Eq. (22), the quantum HHG amplitude can be expressed in the form

$$A_j(\Omega) = -ie^{-i\boldsymbol{K}_\Omega\cdot\boldsymbol{X}_j}N_\Omega\boldsymbol{\epsilon}_\Omega\cdot\int_{-\infty}^{\infty} dt e^{i\Omega t}\boldsymbol{D}_{i,i}(t). \tag{24}$$

Thus, the quantum HHG amplitude is clearly *proportional* to the Fourier transform (FT) of the expectation value of the transition dipole operator, Eq. (23). We may recall that the proportionality constant N_Ω above is of quantum electrodynamical origin and *cannot* be derived from the classical electrodynamics alone [34].

In practice, the FT of interest can be conveniently obtained by fast Fourier transform (or FFT) numerically [35]. Alternatively, for "slowly varying" pulse envelopes (compared to the high-order harmonic frequency) one may express the FT of $\boldsymbol{D}_{i,i}(t)$ as a Fourier series [28],

$$\boldsymbol{D}_{i,i}(t) = \sum_n e^{-in(\omega t - \boldsymbol{k}_\omega\cdot\boldsymbol{X}_j)}\tilde{\boldsymbol{D}}(n\omega), \tag{25}$$

where $\tilde{\boldsymbol{D}}(n\omega)$ is the FT evaluated at the nth harmonic frequency $\Omega = n\omega$. Thus, in terms of the FT components, the HHG amplitude $A_j(\Omega)$ becomes

$$A_j(\Omega) = \sum_n -2\pi i\delta(\Omega - n\omega)e^{-i(\boldsymbol{K}_\Omega - n\boldsymbol{k}_\omega)\cdot\boldsymbol{X}_j} \times N_\Omega\boldsymbol{\epsilon}_\Omega\cdot\tilde{\boldsymbol{D}}_{i,i}(n\omega), \tag{26}$$

where we have carried out the time integration over dt, using the Dirac δ function.

C. Coherent sum of HHG amplitudes: Many-molecule versus one-molecule signal

It is interesting also to consider the *total* amplitude $A_{\mathrm{tot}}(\Omega)$ of HHG emission from all the molecules interacting with the (probe laser) field. This is given by the *coherent* sum of the individual amplitudes emitted by the molecules at the positions $\boldsymbol{X}_j$ for all $j = 1, 2, 3, \ldots, \mathcal{N}$, where $\mathcal{N}$ is the number of molecules in the interaction volume, or

$$\begin{aligned}A_{\mathrm{tot}}(\Omega) &\equiv \sum_{j=1}^{\mathcal{N}} A_j(\Omega) = \sum_n \left\{\sum_{j=1}^{\mathcal{N}} e^{-i(\boldsymbol{K}_\Omega - n\boldsymbol{k}_\omega)\cdot\boldsymbol{X}_j}\right\}_1 \\ &\quad \times \left\{-2\pi i\sum_n \delta(\Omega - n\omega)T_{i,i}(\Omega)\right\}_2\end{aligned} \tag{27}$$

where we may identify the basic HHG transition matrix element for the emission of the nth harmonic per molecule as

$$T_{i,i}(\Omega) = N_\Omega \boldsymbol{\epsilon}_\Omega \cdot \tilde{\boldsymbol{D}}_{i,i}(\Omega). \tag{28}$$

It can be seen from Eq. (27) that the nth harmonic emission amplitude in fact factorizes into two parts: the first factor corresponds to the sum of the macroscopic space-dependent phases associated with the random positions $\boldsymbol{X}_j$ of the C.M.'s of the molecules in the interaction volume, and the second factor corresponds to the fundamental "one-molecule" emission amplitude, independent of the position of the C.M.'s of the molecules. The macroscopic phase factor is explicitly given by

$$\{\cdots\}_1 \equiv \left\{ \sum_{j=1,\mathcal{N}} e^{-i(\boldsymbol{K}_\Omega - n\boldsymbol{k}_\omega)\cdot \boldsymbol{X}_j} \right\}_1. \tag{29}$$

For a large number of molecules in the interaction volume, $\mathcal{N} \gg 1$, the phase factor oscillates greatly and thus tends to average out to zero, *except* when the condition

$$(\boldsymbol{K}_\Omega - n\boldsymbol{k}_\omega) = 0 \tag{30}$$

is fulfilled; in that case, it yields the phase sum $\{\cdots\}_1 = \mathcal{N}$. It is readily understood that the condition (30) corresponds exactly to the momentum conservation between the final momentum of the emitted harmonic photon, $\hbar \boldsymbol{K}_\Omega$, and the sum of the momenta of n laser photons, $n\hbar \boldsymbol{k}_\omega$. This is the phase-matching condition in the forward direction [37].

The probability of emission of the harmonics is given as usual by the absolute square of the total amplitude Eq. (27). Under the phase-matching condition, the latter is therefore coherently *amplified* by a (generally large) factor of $\mathcal{N}^2$. This is also the origin of the *quadratic* pressure dependence of the high-order harmonic signals, as well as their unusual strengths, that had been found in the very first experimental observations (e.g., [38,39]).

The second factor $\{\cdots\}_2$ gives the fundamental "one-molecule" quantum emission amplitude. We also note that if the absolute probability of the harmonic emission is needed, then the proportionality factor $N_\Omega = \sqrt{\frac{2\pi\hbar\omega}{L^3}}$ becomes essential, and that for a given polarization direction of the emitted photon, $\boldsymbol{\epsilon}_\Omega$, the projection of the dipole expectation value must be taken in that direction.

D. Continuous medium and the phase-matching function

If one assumes that the gas molecules are distributed effectively continuously with a distribution function $\mathcal{N}\rho(\boldsymbol{R})d^3R$, where $\rho(\boldsymbol{R})$ is the so-called "density function per molecule," then one may replace the sum over j in Eq. (29) by the integration over the interaction volume. Clearly, in this case the square of the macroscopic phase factor, $|[\cdots]_1|^2$, takes the form

$$|[\cdots]_1|^2 = \mathcal{N}^2 \mathcal{F}(\boldsymbol{K}_\Omega - n\boldsymbol{k}_\omega), \tag{31}$$

where

$$\mathcal{F}(\boldsymbol{K}_\Omega - n\boldsymbol{k}_\omega) = \left| \int d^3X \rho(\boldsymbol{X}) e^{i(\boldsymbol{K}_\Omega - n\boldsymbol{k}_\omega)\cdot \boldsymbol{X}} \right|^2, \tag{32}$$

which is the so-called phase-matching function. It peaks for its argument near zero (near the forward direction), but falls off rapidly away from it.

E. Coherent elastic versus incoherent inelastic transitions

Equations (30) and (27) show, respectively, that both the phase-matching condition (momentum conservation) and the frequency-matching condition (energy conservation) in the process ought to be fulfilled *simultaneously* in order for the macroscopic signal to be coherently amplified in space and time. As already noted, the former condition leads to the directional coherence (forward propagation) of the HHG emission, while the latter implies the *elastic* nature of the accompanying molecular transitions for which the final ("recombination") state f of the molecular system is the *same* as the initial state i, with $E_i = E_f$. In contrast, for an *inelastic* transition, $i \to f$, when $E_i \neq E_f$, there would be in general only "hyper-Raman" emissions, with frequencies $\Omega'_{if} = (n\omega - |E_i - E_f|)$, that are generally incommensurate with the incident laser frequency or its multiple, or the HHG frequency, $\Omega = n\omega$. Thus the nonvanishing relative phase difference $\Delta\phi \equiv (|E_i - E_f| - n\omega)t$ would fail to stimulate the hyper-Raman transitions by the incident field, unlike the stimulated spontaneous nature of the associated HHG. Also the nonvanishing momentum difference between hyper-Raman radiation and the harmonic photon, $\boldsymbol{K}_{\Omega_{if}} - n\boldsymbol{k}_\omega \neq \boldsymbol{0}$, makes the former macroscopically and directionally incoherent.

Finally, we note that the probability of the electronically inelastic processes associated with the transitions into the continuum (e.g., ionization) or between continua (e.g., inverse bremsstrahlung [40]) that are commensurate with the emission of the nth harmonic at the "one-molecule" level will be incoherent spatially, and therefore would enhance only proportional to the total number of molecules, $\mathcal{N}$, in the interaction volume. This is in stark contrast to the coherent amplification of the HHG emission at the nth harmonic, which is proportional to $\mathcal{N}^2$.

F. Differential rate of coherent high-order harmonic generation

To derive the explicit expression for the probability of HHG per unit time, i.e., the *rate* of generation of coherent high-order harmonics, we take the absolute square of the total HHG amplitude, Eq. (27), and divide by the long observation time T, use a useful representation of the square of the δ function [[2], p. R12],

$$\delta^2(\Omega - n\omega) = \lim_{T\to\infty} \frac{T}{2\pi} \delta(\Omega - n\omega), \tag{33}$$

and sum over the emitted photon modes (with $\Sigma_{\boldsymbol{K}_\Omega} \equiv L^3 \int d\hat{\boldsymbol{K}}_\Omega \int dK_\Omega K_\Omega^2$) and get

$$W(\Omega) = \lim_{T\to\infty} \sum_{\boldsymbol{K}} \frac{|A_{\text{tot}}(\Omega)|^2}{T} = \mathcal{N}^2 \sum_n \int d\hat{\boldsymbol{K}}_\Omega \mathcal{F}(\boldsymbol{K}_\Omega - n\boldsymbol{k}_\omega) \times \int dW(n\omega), \tag{34}$$

where

$$dW(n\omega) = 2\pi\delta(\Omega - n\omega)L^3 \times |N_\Omega \boldsymbol{\epsilon}_\Omega \cdot \tilde{\boldsymbol{D}}_{i,i}(n\omega)|^2 K_\Omega^2 dK_\Omega \tag{35}$$

is the differential rate of HHG per molecule. Noting that the main contribution arises from the phase-matching condition along the forward direction, we may carry out the mode integrations to get

$$W(n\omega) = 2\pi |T_{i,i}^{(n)}|^2 \frac{(n\omega)^2}{c^3}, \tag{36}$$

where we have used $K_\Omega \equiv \frac{\Omega}{c}$, $\boldsymbol{K}_\Omega \equiv K_\Omega \hat{\boldsymbol{K}}_\Omega$, and the fundamental transition matrix element for the emission of the nth harmonic, $T_{i,i}^{(n)}$, is given in terms of the FT of the dipole expectation value $\tilde{\boldsymbol{D}}_{i,i}(n\omega)$ by

$$T_{i,i}^{(n)} = \sqrt{2\pi(n\omega)}\boldsymbol{\epsilon}_\Omega \cdot \tilde{\boldsymbol{D}}_{i,i}(n\omega) \tag{37}$$

for $L^3|N_\Omega|^2 = 2\pi(n\omega)$.

IV. EVALUATION OF "ONE-MOLECULE" HHG AMPLITUDE

Clearly the dynamical properties of the HHG signal are given by the rate of HHG emission per molecule, Eq. (36), while the total signal is the same to within a proportionality constant given by the square of the number of molecules in the interaction volume, $\mathcal{N}^2$, and the phase-matching constant $\int d\hat{\boldsymbol{K}}_\Omega \mathcal{F}(\boldsymbol{K}_\Omega - n\boldsymbol{k}_\omega)$ that peaks in the forward direction. We therefore proceed to evaluate the dynamical signal per molecule (in a relative scale) as follows: (i) solve the Schrödinger equation for the nuclear and the electronic motions of the interacting laser-molecule system, (ii) construct a complete set of orthonormal reference states, $|i\rangle \equiv |\chi_i(t)\rangle$, of the molecule, created by the pump pulse, (iii) determine their statistical weights according to the *one-to-one* correspondence with the thermally occupied rotational eigenstates of the ensemble, (iv) calculate the "one molecule" probability amplitude for HHG for each member of the ensemble of linearly independent reference states $|i\rangle$, using Eq. (36), and finally, (v) obtain the (scaled) signal "per molecule" by thermally averaging the *probabilities* of HHG emission from each member of the ensemble of the reference states, using the distribution of their statistical weights.

In the Born-Oppenheimer approximation and nonoverlapping pump and probe pulse condition, we may consider the evolution of the wave functions of the nuclear and the electronic parts separately and combine them together to obtain the wave function of the interacting system to evaluate the transition matrix elements of interest.

A. Pump-pulse interaction and rotational wave packets as reference states

The nuclear rotational motion under the action of the pump pulse is determined by the Schrödinger equation governed by the partial Hamiltonian,

$$H_N(t) + V_{N\text{-}L1}(t), \tag{38}$$

i.e.,

$$i\frac{\partial}{\partial t}|\Phi_{JM}(t)\rangle = [H_N + V_{N\text{-}L_1}(t)]|\Phi_{JM}(t)\rangle. \tag{39}$$

We first construct the fundamental set of linearly independent solutions of Eq. (39), each evolving independently from each of the occupied rotational eigenstates $\{|J_0M_0\rangle\}$. We expand it on the basis of the eigenstates $\{|JM\rangle\}$ as

$$|\Phi_{J_0M_0}(t)\rangle = \sum_{JM} C_{JM}^{(J_0M_0)}(t)|JM\rangle e^{-iE_{JM}t}. \tag{40}$$

The coefficients $C_{JM}^{(J_0M_0)}(t)$ satisfy the system of coupled linear differential equations

$$i\frac{\partial}{\partial t}C_{JM}^{(J_0M_0)}(t) = \sum_{J'M'} \langle JM|V_{N\text{-}L_1}(t)|J'M'\rangle \times e^{i(E_{JM}-E_{J'M'})t} C_{J'M'}^{(J_0M_0)}(t). \tag{41}$$

This set of equations can be easily obtained (e.g., [41]) by projecting on a given eigenstate from the left. In practice, we obtain the fundamental set of solutions $|\Phi_{J_0M_0}(t)\rangle$ by numerical integration, using the well-known Runge-Kutta method [35], starting with the following independent initial conditions:

$$C_{JM}^{(J_0M_0)}(t_i) = \delta_{J,J_0}\delta_{M,M_0}. \tag{42}$$

We may note explicitly here that (a) each independent wave-packet state $|\Phi_{J_0M_0}(t)\rangle$ evolves in *one-to-one* correspondence with the initially occupied rotational eigenstate $|J_0M_0\rangle$. Taken together, they form a complete set of orthonormal rotational wave-packet states (linear superposition of rotational eigenstates),

$$\sum_{J_0M_0} |\Phi_{J_0M_0}(t)\rangle\langle\Phi_{J_0M_0}(t)| = \mathbf{1}. \tag{43}$$

In general, a gas jet of molecules in a pump-probe experiment at a finite temperature T is not in a pure quantum state but rather is in a state of thermal mixture of the rotational eigenstates, $\{|J_0M_0\rangle\}$. We therefore introduce the quantum statistical mechanical device of a hypothetical ensemble of mutually independent and identical reference molecules, each of which occupies the electronic ground state and the rotational eigenstates $\{|J_0M_0\rangle\}$, the latter with statistical weights $\rho(J_0M_0)$, given by the Boltzmann distribution,

$$\rho(e,J_0M_0) = (1)_e Z_P e^{-E_{J_0M_0}/kT}, \tag{44}$$

where

$$Z_P = \sum_{J_0} (2J_0+1)e^{-E_{J_0}/kT} \tag{45}$$

is the rotational partition function; $E_{J_0M_0} = J_0(J_0+1)hBc$, for all M_0; B stands for the rotational constant. We shall assume for the present purpose that the pump pulse is not too strong so that the change in the occupation probability of the ground electronic state after the pump pulse interaction is negligible and hence the ground electronic state at a time t before the interaction with the probe pulse evolves simply to $|\phi_e(t)\rangle = e^{-iE_e t}|\phi_e(0)\rangle$, where E_e is the ground-state energy. [We may assume that electronically only the ground elec-

tronic state $|\phi_e(0)\rangle$ is occupied initially.] Thus, the linearly independent reference states of the molecule, after the interaction of the pump pulse and immediately before the interaction with the probe pulse, can be written as the direct product of the nuclear rotational wave-packet states and the electronic ground state,

$$|\chi_i(t)\rangle \equiv |\Phi_{J_0M_0}(t)\rangle|\phi_e(t)\rangle, \quad i \equiv (e,J_0M_0). \tag{46}$$

The reference density matrix describing the molecular ensemble prepared by the pump pulse takes the form

$$\rho_{\rm mol}(e,J_0M_0) = \sum_i |\chi_i(t)\rangle\rho(e,J_0M_0)\langle\chi_i(t)| = |\phi_e(t)\rangle|\Phi_{J_0M_0}(t)\rangle\rho(j_0M_0) \times \langle\Phi_{J_0M_0}(t)|\langle\phi_e(t)|, \tag{47}$$

where $i \equiv (e,J_0M_0)$. The above ensemble of states describes the effective "initial" condition of the system after the pump pulse when the probe pulse arrives at the molecule at $\boldsymbol{X}_j$. To avoid any possible confusion regarding the presence of the ensemble of "mixed states," and the "rotational coherence," we may already point out explicitly that while the ensemble at a given point in space is characterized by the statistical occurrence of the reference states $\{|\chi_{i=e,J_0M_0}(t)\rangle\}$, each one of the reference states carries the information of the rotational coherence (induced by the pump pulse) and coded in the rotational wave packets $\{|\Phi_{J_0M_0}(t)\rangle\}$ of the reference states. Thus, the thermal average of the HHG emission signal that must be taken with respect to the *probability* of emission from each member of the ensemble (as required by quantum statistical mechanics) cannot, and will not, wash out the rotational coherence encoded in each of the reference states individually.

B. Interaction with probe-pulse and evolution of the electronic state

To proceed further, we next consider the time evolution of the electronic state, governed by the partial Hamiltonian

$$H_e + V_{e\text{-}L_2}(t-t_d). \tag{48}$$

It is obtained conveniently from the knowledge of the electronic Green's function $G_e(t,t')$ [20] associated with the above Hamiltonian, and defined by the inhomogeneous equation

$$\left\{ i\frac{\partial}{\partial t} - [H_e + V_{e\text{-}L_2}(t-t_d)] \right\} G_e(t,t') = \delta(t-t')\mathbf{1}. \tag{49}$$

A solution of the above equation can be written (in the strong-field KFR-approximation) as

$$G_e(t,t') = -i\theta(t-t')\sum_{j,\boldsymbol{p}} |\phi_j^{(+)}\rangle e^{-iE_j^+ t}|\boldsymbol{p}(t-t_d)\rangle \times e^{-(i/2)\int_{t'-t_d}^{t-t_d} p^2(u)du} \times \langle \boldsymbol{p}(t'-t_d)|e^{iE_j^+ t'}\langle\phi_j^{(+)}|, \tag{50}$$

where j runs over all the intermediate ionic electronic states $|\phi_j^{(+)}\rangle$, with eigenvalues E_j^+; $\boldsymbol{p}$ is the free momentum of the continuum electron, and $\boldsymbol{p}(t)$ stands for the instantaneous momentum in the presence of the field, $\boldsymbol{p}(t) \equiv (\boldsymbol{p} + \frac{\boldsymbol{A}(t)}{c})$. The validity of Eq. (50) can be verified by substituting it in Eq. (49) and using the completeness relation

$$\sum_{\boldsymbol{p}} \langle \boldsymbol{r}|\phi_{\boldsymbol{p}}(t)\rangle\langle\phi_p(t)|\boldsymbol{r}\rangle = \mathbf{1} \tag{51}$$

of the Volkov wave functions defined by

$$\langle \boldsymbol{r}|\phi_{\boldsymbol{p}}(t)\rangle = e^{i\boldsymbol{p}(t)\cdot\boldsymbol{r}} e^{-(i/2)\{\int^t [p^2(u)]du\}} \tag{52}$$

as well as the completeness relation of the molecular ionic states

$$\sum_j |\phi_j^{(+)}\rangle\langle\phi_j^{(+)}| = 1. \tag{53}$$

We should note that the ionic states are generally much more tightly bound than the active electron in the highest occupied molecular orbital (HOMO). Thus in deriving G_e above, we have further neglected the change in the ionic states due the interaction with the probe pulse, which we may refer to as a "bare-ion" approximation.

Finally, using Eqs. (43) and (50) we obtain the total Green's function $G_0(t,t')$ of the interacting system,

$$G_0(t,t') = -i\theta(t-t')\sum_{j\boldsymbol{p}JM} |\phi_j^{(+)}\rangle|\phi_{\boldsymbol{p}}(t-t_d)\rangle \times |\Phi_{JM}(t)\rangle e^{-iE_j^+(t-t')}\langle\Phi_{JM}(t')| \times \langle\phi_{\boldsymbol{p}}(t'-t_d)|\langle\phi_j^{(+)}|. \tag{54}$$

The above Green's function (54) therefore holds under (a) the adiabatic Born-Oppenheimer, (b) the strong-field KFR, and (c) the "bare-ion" approximations.

C. The total wave function in the strong-field molecular KFR approximation

Combining Eqs. (17) and (46), we obtain the intense-field molecular wave function,

$$|\Psi_i(t)\rangle = |\chi_i(t)\rangle + \int_{-\infty}^{\infty} dt' \times G_0(t,t')V_{e\text{-}L_2}(t'-t_d)|\chi_i(t')\rangle, \tag{55}$$

where

$$|\chi_i(t)\rangle = |\phi_e(t)\rangle|\Phi_{J_0M_0}(t)\rangle \tag{56}$$

is a member of the ensemble of reference states of interest.

D. Evaluation of the dipole expectation value

In the above, we have obtained the necessary ingredients for evaluating the expectation of the dipole operator, Eq. (23), explicitly. Substituting Eqs. (54) and (55) in Eq. (23), we get

$$\boldsymbol{D}_{i,i}(t) = \langle \chi_i(t)|\hat{\boldsymbol{d}}_e|\Psi_i^{(1)}(t)\rangle + \text{c.c.} = \left\{ -i\int_{-\infty}^{t} dt' \langle \phi_e(t)| \times \langle \Phi_{J_0M_0}(t)|\hat{\boldsymbol{d}}_e \times \sum_{jpJM} |\phi_j^{(+)}\rangle|\phi_{\boldsymbol{p}}(t-t_d)\rangle \times |\Phi_{JM}(t)\rangle e^{-iE_j^+(t-t')}\langle \Phi_{JM}(t')| \times \langle \phi_{\boldsymbol{p}}(t'-t_d)|\langle \phi_j^{(+)}| \times V_{e\text{-}L_2}(t'-t_d)|\Phi_{J_0M_0}(t')\rangle|\phi_e(t')\rangle \right\} + \text{c.c.} \quad (57)$$

To simplify it further, (i) we change the variables $t' \to t' + t_d$ and $t \to t + t_d$; (ii) we note that the free evolution of a rotational wave packet after the interaction with the pump pulse at $(t+t_d)$ is $\Phi_{J_0M_0}(t+t_d) = e^{-iH_Nt}\Phi_{J_0M_0}(t_d)$, and, similarly, at $(t'+t_d)$, it is $\Phi_{J_0M_0}(t'+t_d) = e^{-iH_Nt'}\Phi_{J_0M_0}(t_d)$; and (iii) we note that the time dependence of the upper-turbed initial electronic state at $\phi_e(t+t_d) = |\phi_e\rangle e^{-iE_i(t+t_d)}$, and similarly for the ionic states, $\phi_j^{(+)}(t+t_d) = |\phi_j^{(+)}\rangle e^{-iE_j^+(t-t_d)}$; (iv) we introduce the overlaps (or "Dyson orbitals"),

$$|\phi_e^{(j)}\rangle = \langle \phi_j^{(+)}(1,2,\ldots,N_e-1)|\phi_e(1,2,\ldots,N-1,N)\rangle; \quad (58)$$

and (v) we retain only the (dominant) contribution from the lowest-lying intermediate ionic state ($j=0$), to obtain

$$\boldsymbol{D}_{i,i}(t) = -i\sum_{jJM,\boldsymbol{p}} \langle \Phi_{J_0M_0}(t)|\langle \phi_e^{(0)}|\hat{\boldsymbol{d}}_e| \times |\boldsymbol{p}(t-t_d)\rangle|\phi_j^+\rangle|\Phi_{JM}(t)\rangle \times \int_{-\infty}^{t} dt' e^{-i(E_j^+ - E_0)(t-t')} \times e^{-i\int_{t'-t_d}^{t-t_d}(\boldsymbol{p}(u)^2/2)du} \times \langle \Phi_{JM}(t')|\langle \phi_j^+|\langle \boldsymbol{p}(t'-t_d)| \times |V_{e\text{-}L_2}(t'-t_d)|\phi_e^{(0)}\rangle \times |\Phi_{J_0M_0}(t')\rangle + \text{c.c.} \quad (59)$$

Or

$$\boldsymbol{D}_{i,i}(t) = \langle \Phi_{J_0M_0}(t)|\boldsymbol{D}_e(t)|\Phi_{J_0M_0}(t)\rangle, \quad (60)$$

with the electronic part of the expectation value

$$\boldsymbol{D}_e(t) = \left\{ -i\sum_{\boldsymbol{p}} \langle \phi_e^{(0)}|\hat{\boldsymbol{d}}_e|\boldsymbol{p}(t)\rangle \times \int_{-\infty}^{t_d+t} dt' e^{-i\int_{t'}^{t}[\boldsymbol{p}(u)^2/2+E_B]du} \times \langle \boldsymbol{p}(t')|-\boldsymbol{F}(t')\cdot\hat{\boldsymbol{d}}_e|\phi_e^{(0)}\rangle \right\} + \text{c.c.}, \quad (61)$$

where $\boldsymbol{F}(t)$ is the probe field. Finally, by using the rate of emission of the nth harmonic as given by Eq. (36), we obtain the dynamic HHG signal, for a pump-probe delay time t_d,

$$S^{(n)}(t_d,\alpha) = 2\pi\sum_{J_0M_0} \rho(J_0)|\langle \Phi_{J_0M_0}(t_d)|T_e^{(n)}(\theta,\phi;\alpha)| \times |\Phi_{J_0M_0}(t_d)\rangle|^2 \frac{(n\omega)^2}{c^3}, \quad (62)$$

where $(\theta,\phi) \equiv \hat{\boldsymbol{R}}_N$ is the direction of the molecular axis in space, and $T_e^{(n)}(\theta,\phi;\alpha)$ is the electronic part of the *HHG transition operator* for a given orientation of the molecular axis and a relative polarization angle α.

E. Derivation of the HHG operator $T^{(n)}(\theta,\phi;\alpha)$

We shall now proceed to derive an explicit expression of the HHG transition operator $T_e^{(n)}(\theta,\phi;\alpha)$ or equivalently (to within a constant) the transition dipole expectation value $D_e(t_d)$. To this end, we first consider the most common experimental geometry in which the pump and probe polarizations are chosen to be parallel.

1. HHG operator: Parallel polarization $\alpha=0$

We recall that for a linearly polarized probe pulse $\boldsymbol{F}_2(t) = \hat{\boldsymbol{\epsilon}}_{\boldsymbol{\Omega}}F(t)\cos\omega t$, the corresponding vector potential is

$$\boldsymbol{A}(t) = -\hat{\boldsymbol{\epsilon}}_{\Omega}\left(\frac{cF(t)}{\omega}\right)\sin\omega t. \quad (63)$$

It is convenient in this case to take the space fixed polar axis (z axis) along the common direction of the polarizations $\boldsymbol{\epsilon}_1 \| \boldsymbol{\epsilon}_2 \| \hat{\boldsymbol{z}}$. To evaluate the triple-integral over the intermediate momenta $\boldsymbol{p}$ in Eq. (61), we employ the stationary phase method [42], with the stationary values

$$\boldsymbol{p}_{\text{st}}(t,t') = \frac{1}{t-t'}\int_{t'}^{t} \boldsymbol{A}(t'')dt'', \quad (64)$$

for which the derivative of the action $S(t,t')$ with respect to $t' = t-\tau$ is equal to zero. The corresponding stationary value of the action is

$$S_{\text{st}}(t,t') = \int_{t'}^{t}\left\{\frac{1}{2}\left(\boldsymbol{p}_{\text{st}}(t,t'') - \frac{1}{c}\boldsymbol{A}(t'')\right)^2 + E_B\right\}dt'', \quad (65)$$

where $\boldsymbol{p}(t) = \boldsymbol{p}_{\text{st}}(t,t') - \frac{1}{c}\boldsymbol{A}(t)$ and $\boldsymbol{p}(t') = \boldsymbol{p}_{\text{st}}(t,t') - \frac{1}{c}\boldsymbol{A}(t')$. Thus, projecting the resulting value of $D_e(t)$ on to the polarization direction $\boldsymbol{\epsilon}_{\Omega}$ of the emitted harmonic, we get

$$D_e(t) = \left\{ i\int_0^t dt' \left(\frac{\pi}{\varepsilon + i(t-t')/2}\right)^{3/2} \times \langle \phi_e^{(0)}|\varepsilon_{\Omega}\cdot\boldsymbol{r}|\boldsymbol{p}(t)\rangle e^{-iS_{\text{st}}(t,t')} \times \langle \boldsymbol{p}(t')|\boldsymbol{F}(t')\cdot\boldsymbol{r}|\phi_e^{(0)}\rangle \right\} + \text{c.c.} \quad (66)$$

We may note that the first matrix element in this expression (reading from the right to the left) corresponds to the "ionization" transition at time t', $d_{\text{ion}}(t') \equiv \langle \boldsymbol{p}(t')|\boldsymbol{F}(t')\cdot\boldsymbol{r}|\phi_e^{(0)}\rangle$, whereas the last matrix element corresponds to a "recombination" transition of the electron to the same initial state at a time t, or $d_{\text{rec}}(t) \equiv \langle \phi_e^{(0)}|\boldsymbol{\epsilon}_{\Omega}\cdot\boldsymbol{r}|\boldsymbol{p}(t)\rangle$. The interval $(t-t')$ corresponds to the intermediate time that the electron spends in the continuum Volkov states, between the absorption of n photons from the probe pulse and the emission of the harmonic photon of frequency $\Omega = n\omega$. We have assumed that the depletion of the ground-state population during the process is negligible. However, if needed, a weak depletion due to ionization could be accounted for without difficulty by introducing in the above expression an exponential decay factor: $e^{-(\gamma/2)(t+t')}$, where γ is the total ionization rate.

2. The "ionization" and "recombination" matrix elements

To evaluate the matrix elements of "ionization" and "recombination" in Eq. (66), we assume that the wave function of the active electron may be given by the highest occupied molecular orbital. (If needed, other occupied orbitals can be considered analogously.) It can be written either in the multicenter LCAO-MO form, or we may transform it into an equivalent single-center MO (e.g., [43,44]). It is useful also to note that in the latter form, it often suffices for problems of interaction of molecules with long-wavelength laser fields (preferably in conjunction with the "length gauge") to retain only the asymptotic form of the orbitals at distances away from the molecular center. Let the unperturbed MO of the active electron of a linear molecule be given in the body fixed frame by the single-center expansion,

$$\phi_e^{(0)}(\boldsymbol{r}) = \sum_l C_l^{(m)} R_l(r) Y_{lm}(\hat{\boldsymbol{r}}), \tag{67}$$

where $C_l^{(m)}$ are the expansion coefficients, $R_l(r)$ are the radial waves of angular momentum l, $Y_{lm}(\hat{\mathbf{r}})$ are the spherical harmonics, and m is the conserved projection quantum number of the angular momentum, l, of the active electron, along the molecular axis.

Next, we transform the molecular orbitals, Eq. (67), from the body fixed frame to the space fixed frame, using the Wigner transformation $\boldsymbol{D}$,

$$\phi_e^{(0)}(\boldsymbol{r}) = \hat{\boldsymbol{D}}\phi_e^{(0)}(\boldsymbol{r}) = \sum_l C_l^{(m)} R_l(r) \times \sum_\mu D_{\mu m}^l(\phi,\theta,\chi) Y_{l\mu}(\hat{\boldsymbol{r}}). \tag{68}$$

Above, $D_{\mu m}^l(\phi,\theta,\chi) = e^{-i\mu\phi} d_{\mu m}^l(\theta) e^{-im\chi}$ is the Wigner rotation matrix where (ϕ,θ,χ) are Euler's angles, which define the orientation of the molecular axis to the space fixed coordinate frame (e.g., [45]). The middle term of the Wigner matrix, $d_{\mu m}^l(\theta)$, has been tabulated, e.g., in Refs. [45,46]. The matrix element of the dipole along the direction of the probe pulse, appearing in Eq. (66), then reads

$$d_{\text{ion}}(t') = F(t') \sum_l C_l^{(m)} \sum_\mu D_{\mu m}^l(\phi,\theta,\chi) \times \langle e^{i\boldsymbol{p}_{t'}\cdot\boldsymbol{r}} | \boldsymbol{\epsilon}_\omega \cdot \boldsymbol{r} | R_l(r) Y_{l\mu}(\hat{\boldsymbol{r}}) \rangle. \tag{69}$$

Further, we expand $e^{-i\boldsymbol{p}_{t'}\cdot\boldsymbol{r}}$ in spherical harmonics,

$$e^{-i\boldsymbol{p}_{t'}\cdot\boldsymbol{r}} = \frac{(2\pi)^{3/2}}{\sqrt{p_{t'} r}} \sum_{l'm'} (-i)^{l'} J_{l'+1/2}(p_{t'} r) \times Y_{l'm'}(\hat{\boldsymbol{p}}_{t'}) Y_{l'm'}^*(\hat{\boldsymbol{r}}), \tag{70}$$

and note that in this system of axes we have

$$\boldsymbol{\epsilon}_\omega \cdot \boldsymbol{r} = r\sqrt{\frac{4\pi}{3}} Y_{10}(\hat{\boldsymbol{r}}). \tag{71}$$

We note also that the stationary instantaneous momentum $\boldsymbol{p}_{t'}$ can be either parallel or antiparallel with respect to the direction of the field so that $\theta_{p_t}=0$, π and $\phi_{p_t}=0$. Therefore, the spherical harmonics with the argument $\hat{\boldsymbol{p}}_{t'}$ can be simplified to $Y_{l'm'}(\hat{\boldsymbol{p}}_{t'}) = (\sigma)^{l'}\sqrt{\frac{2l'+1}{4\pi}}\delta_{m',0}$, with $\sigma=1$ for $\theta_{p_t}=0$ and $\sigma=-1$ for $\theta_{p_t}=\pi$. Substituting Eqs. (70) and (71) in Eq. (69), we obtain (with $l=l_i$ for the initial bound state in the "ionization" matrix element)

$$d_{\text{ion}}(t') = F(t') \frac{(2\pi)^{3/2}}{\sqrt{3p_{t'}}} \sum_{l_i,l',\mu} C_{l_i}^{(m)} D_{\mu m}^{l_i}(\phi,\theta,\chi) \times (-i\sigma)^{l'} \sqrt{(2l'+1)} \langle l'0|10|l_i\mu\rangle I_{l_i,l'}(t'), \tag{72}$$

where we have defined the radial integrals (m fixed) by

$$I_{l_i,l'}(t') = \int_0^\infty J_{l'+(1/2)}(p_{t'} r) R_{l_i}(r) r^{-1/2} r r^2 dr. \tag{73}$$

The Clebsch-Gordan coefficient in Eq. (72) implies that only the terms with $\mu=0$ and $l'=l\pm1$ survive in the sums (e.g., [45,46])

$$\langle l'0|10|l_i\mu\rangle = \begin{cases} \left(\frac{3}{4\pi}\right)^{1/2}\left(\frac{l_i+1}{\sqrt{(2l_i+3)(2l_i+1)}}\right)\delta_{l'l_i+1}\delta_{0\mu} \\ \left(\frac{3}{4\pi}\right)^{1/2}\left(\frac{l_i}{\sqrt{(2l_i+1)(2l_i-1)}}\right)\delta_{l'l_i-1}\delta_{0\mu}. \end{cases} \tag{74}$$

Thus, for the "ionization dipole," we get

$$d_{\text{ion}}(t') = F(t') \sum_{l_i} C_{l_i}^{(m)} D_{0m}^{(l_i)}(\phi,\theta,\chi) \beta_{\text{ion}}(l_i,m;t') \tag{75}$$

with

$$\beta_{\text{ion}}(l_i,m;t') = \frac{2\pi}{\sqrt{2p_{t'}}} \frac{1}{\sqrt{(2l_i+1)}} \times [(-i\sigma)^{l_i+1}(l_i+1) I_{l_i,l_i+1}(t') + (-i\sigma)^{l_i-1} l_i I_{l_i,l_i-1}(t')]. \tag{76}$$

Using the Slater-orbital representation of the single center radial functions, $R_l(r) = r^{\eta-1}e^{-p_B r}$, with $\eta \equiv Z_c/p_B$, Z_c is the core charge, and $p_B = \sqrt{2|E_B|}$ with E_B the binding energy, the radial integrals (I's) appearing in d_{ion} [Eq. (72)] can be evaluated explicitly by using the formula [47]

$$\int_0^\infty e^{-\alpha x} J_\nu(\beta x) x^{\mu-1} dx = \frac{\left(\frac{\beta}{2}\right)^\nu \Gamma(\nu+\mu)}{\sqrt{(\alpha^2+\beta^2)^{\nu+\mu}}\Gamma(\nu+1)} \times F\left(\frac{\nu+\mu}{2}, \frac{1-\mu+\nu}{2}, \nu+1; \frac{\beta^2}{\alpha^2+\beta^2}\right), \tag{77}$$

where $F(a,b,c;x)$ is a hypergeometric function. Note that since the argument $x \equiv \frac{\beta^2}{\alpha^2+\beta^2} < 1$, the hypergeometric function is guaranteed to converge for all values of a, b, and c. For the "ionization" step, the radial integration reads

$$I_{l_i,l_i+1}(t') = \frac{\left(\frac{p_{t'}}{2}\right)^{l+3/2} \Gamma(l_i + Z_c/p_B + 4)}{\sqrt{(P_B^2 + p_{t'}^2)^{l_i+Z_c/p_B+4}}\Gamma\left(l_i + \frac{5}{2}\right)} \times F\left(\frac{l_i + Z_c/p_B + 4}{2}, \frac{l_i - Z_c/p_B}{2}, l_i + \frac{5}{2}; \frac{p_{t'}^2}{p_B^2 + p_{t'}^2}\right),$$

$$I_{l_i,l_i-1}(t') = \frac{\left(\frac{p_{t'}}{2}\right)^{l_i-1/2} \Gamma(l_i + Z_c/p_B + 2)}{\sqrt{(p_B^2 + p_{t'}^2)^{l_i+Z_c/p_B+2}}\Gamma\left(l_i + \frac{1}{2}\right)} \times F\left(\frac{l_i + Z_c/p_B + 2}{2}, \frac{l_i - Z_c/p_B - 2}{2}, l_i + \frac{1}{2}; \frac{p_{t'}^2}{p_B^2 + p_{t'}^2}\right). \quad (78)$$

We may assume that the emitted harmonic is observed with its polarization along the same direction as the probe pulse polarization. (There is no difficulty, except lengthier algebra, to obtain the expression for the polarization direction orthogonal to it, but the former would give the dominant contribution under phase-matching condition.) Following an analogous calculation as above, we get the "recombination" matrix element as (with $l=l_r$ for the final bound state in the "recombination" matrix element)

$$d_{\rm rec}(t) = \sum_{l_r} C_{l_r}^{(m)*} D_{0m}^{l_r*}(\phi,\theta,\chi)\beta_{\rm rec}(l_r,m;t') \quad (79)$$

with

$$\beta_{\rm rec}(l_r,m;t) = \frac{2\pi}{\sqrt{2p_t}} \frac{1}{\sqrt{(2l_r+1)}} \times [(i\sigma)^{l_r+1}(l_r+1)I_{l_r,l_r+1}(t) + (i\sigma)^{l_r-1} l_r I_{l_r,l_r-1}(t)]. \quad (80)$$

The radial integrals in Eq. (80) can be evaluated by using Eq. (78), except that l_i is changed to l_r, and t' to t, throughout. Substituting Eqs. (75), (76), (79), and (80) in Eq. (66), we obtain

$$D_e(t) = \sum_{l_i,l_r} d_{0m}^{l_r}(\theta) d_{0m}^{l_i}(\theta) \times [C_{l_r}^{(m)*} C_{l_i}^{(m)} M_e^{(l_r,l_i)}(t) + \text{c.c.}], \quad (81)$$

where we have used the relation

$$D_{0m}^{l_r*}(\phi,\theta,\chi) D_{0m}^{l_i}(\phi,\theta,\chi) = d_{0m}^{l_r}(\theta) d_{0m}^{l_i}(\theta) \quad (82)$$

and defined the radial integral

TABLE I. Explicit form of $d_{0m}^{l}(\theta)$ required for evaluating Eq. (84) [45,46].

l	N_2 $(m=0)$	O_2 $(m=1)$
0	1	
2	$\frac{1}{2}(3\cos^2\theta - 1)$	$\sqrt{\frac{3}{2}}\sin\theta\cos\theta$
4	$\frac{1}{8}(3 - 30\cos^2\theta + 35\cos^4\theta)$	$-\frac{\sqrt{5}}{4}\sin\theta\cos\theta(3-\cos^2\theta)$

$$M_e^{(l_r,l_i)}(t) = i\int_{t_d}^{t_d+t} dt' \left(\frac{\pi}{[\epsilon + i(t-t')/2]}\right)^{3/2} \times \beta_{\rm rec}(l_r,m;t) e^{-iS_{\rm st}(t,t')} \times F(t')\beta_{\rm ion}(l_i,m;t'). \quad (83)$$

Next, by integrating over t', taking the Fourier transform with respect to t, we obtain [cf. Eq. (28)] the HHG operator $T_e^{(n)}(\theta,\phi;0)$ for the nth harmonic generation,

$$T_e^{(n)}(\theta,\phi;0) = \sqrt{2\pi(n\omega)}\tilde{D}_e(n\omega) = \sqrt{2\pi(n\omega)}\sum_{l_i,l_r} d_{0,m}^{l_r}(\theta) d_{0,m}^{l_i}(\theta) \times \tilde{\alpha}_{zz}^{(n)}(l_r,l_i;m), \quad (84)$$

where, $\tilde{\alpha}_{zz}^{(n)}(l_r,l_i;m)$ is given by the nth Fourier coefficient of $D_e(t)$,

$$\tilde{\alpha}_{zz}^{(n)}(l_r,l_i;m) \equiv \mathcal{F}[C_{l_r}^{(m)*} C_{l_i}^{(m)} M_e^{(l_r,l_i)}(t) + \text{c.c.}]_n, \quad (85)$$

where script $\mathcal{F}$ is the Fourier transform. Next, by substituting Eq. (84) in Eq. (62), we obtain the rotational matrix elements,

$$\langle \Phi_{J_0M_0}(t_d) | d_{0m}^{l_r}(\theta) d_{0m}^{l_i}(\theta) | \Phi_{J_0M_0}(t_d) \rangle, \quad (86)$$

which can be evaluated directly by using the tabulated values of the $d_{0m}^{l}(\theta)$ given by elementary trigonometric functions (see Table I). Alternatively, we may first combine the product

$$d_{0m}^{l_r}(\theta) d_{0m}^{l_i}(\theta) = \sqrt{\frac{4\pi}{2l_r+1}}(-1)^m Y_{l_r,-m}(\theta,\phi) \times \sqrt{\frac{4\pi}{2l_i+1}} Y_{l_i,m}(\theta,\phi) = \sum_{L=|l_r-l_i|}^{l_r+l_i} (-1)^m \langle l_r,l_i,-m,m|L,0\rangle \times \langle l_r,l_i,0,0|L,0\rangle P_L(\cos\theta) \quad (87)$$

and we obtain

$$T_e^{(n)}(\theta,\phi;0) = \sum_{l_i,l_r,L} \tilde{a}'^{(n)}_{zz}(l_r,l_i,L;m) P_L(\cos\theta), \quad (88)$$

where

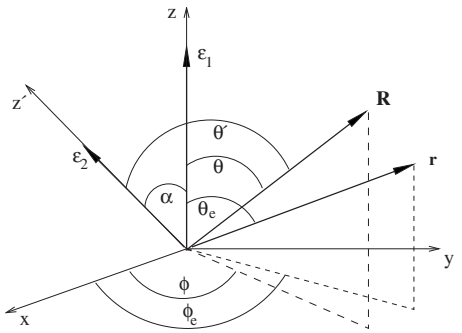

FIG. 3. A schematic diagram defining molecular axis $\boldsymbol{R}$, electron position $\boldsymbol{r}$, pump polarization $\boldsymbol{\epsilon}_1$, and probe polarization $\boldsymbol{\epsilon}_2$; α is the operational laboratory angle.

$$\tilde{a}'^{(n)}_{zz}(l_r,l_i,L;m) = \sqrt{2\pi(n\omega)}\tilde{\alpha}^{(n)}_{zz}(l_r,l_i;m) \times(-1)^m\langle l_r,l_i,-m,m|L,0\rangle \times \langle l_r,l_i,0,0|L,0\rangle. \tag{89}$$

Thus, the expectation value of the transition operator with respect to the rotational wave packet can be obtained more elegantly in terms of the Legendre polynomials moments,

$$\langle P_L\rangle_{J_0M_0}(t_d) \equiv \langle \Phi_{J_0M_0}(t_d)|P_L(\theta)|\Phi_{J_0M_0}(t_d)\rangle. \tag{90}$$

Finally, by substituting the above relations [Eq. (88)] in Eq. (62), and taking the statistical average over the ensemble of the emission probabilities from the ensemble of rotational wave packets, we obtain the HHG signal (i.e., the rate per unit time of generation of the nth harmonic per molecule) in the special case of parallel polarizations (cf. [19]),

$$S^{(n)}(t_d;0) = 2\pi\sum_{J_0M_0}\rho(J_0)\left|\sum_{L,l_r,l_i}\tilde{a}'^{(n)}_{zz}(l_r,l_i,L;m) \times\langle P_L\rangle_{J_0M_0}(t_d)\right|^2\frac{(n\omega)^2}{c^3}. \tag{91}$$

F. General polarization geometry: Arbitrary α

So far we have assumed that the pump and the probe polarizations are parallel and that they point along the space fixed polar axis $\hat{z}$. In the general case, we may define, without loss of generality, the relative angle between the polarizations, α, to lie in the (z,z',x) plane (cf. Fig. 3). From the figure, it can be seen that we simply need to re-express the direction of the molecular axis, (θ,ϕ), given with respect to the pump polarization $\boldsymbol{\epsilon}_1\|\hat{z}$, in terms of the direction (θ',ϕ') with respect to the probe polarization direction $\boldsymbol{\epsilon}_2\|\hat{z}$. This is readily achieved by simply replacing $\cos\theta\rightarrow\cos\theta'$, and using the well known relation

$$\cos\theta' = \cos\alpha\cos\theta + \sin\theta\sin\alpha\cos\phi \tag{92}$$

or the vector addition coefficients and the addition theorem

$$P_L(\cos\theta') = \frac{4\pi}{2L+1}Y_{L,M}(\theta,\phi)Y^*_{L,M}(\alpha,0). \tag{93}$$

Thus, we obtain the general expression of the HHG operator for any α [20],

$$T^{(n)}_e(\theta',\phi';\alpha) = \sqrt{2\pi(n\omega)}\sum_{l_i,l_r} d^{l_r}_{0,m}(\theta')d^{l_i}_{0,m}(\theta') \times \tilde{a}^{(n)}_{zz}(l_r,l_i;m). \tag{94}$$

Or,

$$T^{(n)}_e(\theta',\phi';\alpha) = \sum_{l_r,l_i,L,M}\tilde{a}'^{(n)}_{zz}(l_r,l_i,L;m)P_L(\cos\theta') = \sum_{LM}\sum_{l_r,l_i}\tilde{a}'^{(n)}_{zz}(l_r,l_i,L;m) \times\frac{4\pi}{2L+1}Y_{L,M}(\theta,\phi)Y^*_{L,M}(\alpha,0), \tag{95}$$

where $\tilde{a}'^{(n)}_{zz}(l_r,l_i,L;m)$ is given by Eq. (89).

It should be noted that, in general, if the molecular orbital coefficients were assumed to be complex,

$$C^{(m)}_l \equiv |C^{(m)}_l|e^{i\phi_l}, \tag{96}$$

then we should rewrite the dynamic parameters $\tilde{\alpha}^{(n)}_{zz}(l_r,l_i;m)$ [Eq. (85)] as

$$\tilde{\alpha}^{(n)}_{zz}(l_r,l_i;m) = \mathcal{F}[C^{(m)*}_{l_r}C^{(m)}_{l_i}M^{(l_r,l_i)}_e(t) + \text{c.c.}]_n = 2|C^{(m)}_{l_r}||C^{(m)}_{l_i}| \times[\cos(\phi_{l_il_r})\tilde{u}^{(n)}_{l_r,l_i,m} - \sin(\phi_{l_il_r})\tilde{v}^{(n)}_{l_r,l_i,m}], \tag{97}$$

where

$$\phi_{l_il_r} \equiv (\phi_{l_i} - \phi_{l_r}). \tag{98}$$

$M^{(l_r,l_i)}_e(t)$ is given by Eq. (83), and we have defined

$$\tilde{u}^{(n)}_{l_r,l_i,m} = \mathcal{F}[\text{Re}\{M^{(l_r,l_i)}_e(t)\}]_n, \tag{99}$$

$$\tilde{v}^{(n)}_{l_r,l_i,m} = \mathcal{F}[\text{Im}\{M^{(l_r,l_i)}_e(t)\}]_n. \tag{100}$$

Thus, finally, we can express the general transition matrix element for the nth-order harmonic as an expansion in Legendre polynomials in $\cos\alpha$, and the corresponding Legendre moments of the time-dependent axis distribution of the molecule,

$$T^{(n)}(t_d,\alpha) = \langle\Phi_{J_0M_0}(t_d)|T^{(n)}(\theta,\phi;\alpha)|\Phi_{J_0M_0}(t_d)\rangle = \sum_{L,l_r,l_i}\sqrt{2\pi(n\omega)}[\cos(\phi_{l_il_r})\tilde{u}^{(n)}_{l_i,l_r,m} - \sin(\phi_{l_il_r})\tilde{v}^{(n)}_{l_i,l_r,m}]2|C^{(m)}_{l_r}||C^{(m)}_{l_i}| \times(-1)^m\langle l_r,l_i,-m,m;L,0\rangle \times\langle l_r,l_i,0,0;L,0\rangle \times\langle P_L\rangle_{J_0M_0}(t_d)P_L(\cos\alpha), \tag{101}$$

where we have taken the expectation value of the HHG operator with respect to the rotational wave packet $|\Phi(t_d)\rangle$, to obtain

$$\frac{4\pi}{2L+1}\langle\Phi_{J_0M_0}(t_d)|Y_{LM}(\theta,\phi)|\Phi_{J_0M_0}(t_d)\rangle = \langle P_L\rangle_{J_0M_0}(t_d)P_L(\cos\alpha)\delta_{M,0}. \tag{102}$$

This follows from the observation that the magnetic quantum numbers of all the rotational eigenstates in the individual

wave packets have the same value M_0. It holds when the interaction operator $V_{e\text{-}L_2}(t)$ does not depend on the azimuth angle of the molecular axis in the body fixed frame. In the above expression, we have also used the relation $\sqrt{\frac{4\pi}{2L+1}}Y_{L0}(\theta,\phi)=P_L(\cos\theta)$, and an analogous relation with respect to the angle α, to simplify.

It is useful to note also that, if the orbital expansion coefficients are real, as is often the case, then $\phi_{l_i,l_r}=(0,\pi)$ and therefore the quantity in the square brackets in Eq. (101) simplifies to $[\cdots]=[\cos(\phi_{l_i,l_r})\tilde{u}^{(n)}_{l_r,l_i,m}]$ only.

G. A general formula for the HHG signal

Thus, finally, we substitute Eq. (101) in Eq. (91) and obtain the desired general expression (cf. [20]) for the nth harmonic signal from a linear molecule, for any value of t_d and α,

$$S^{(n)}(t_d,\alpha)=2\pi\sum_{J_0M_0}\rho_{J_0M_0}\left|\sum_{L,l_r,l_i}\sqrt{2\pi(n\omega)}\right.$$
$$\times[\cos(\phi_{l_i,l_r})\tilde{u}^{(n)}_{l_r,l_i,m}-\sin(\phi_{l_i,l_r})\tilde{v}^{(n)}_{l_r,l_i,m}]$$
$$\times 2|C^{(m)}_{l_r}||C^{(m)}_{l_i}|(-1)^m$$
$$\times\langle l_r,l_i,-m,m;L,0\rangle\langle l_r,l_i,0,0;L,0\rangle$$
$$\left.\times\langle P_L\rangle_{J_0M_0}(t_d)P_L(\cos\alpha)\right|^2\frac{(n\omega)^2}{c^3}. \quad (103)$$

We may conclude the section by noting that for the special case of parallel polarizations, $\alpha=0$, $P_L(\cos 0)=P_L(1)=1$, Eq. (103) correctly goes over to the signal obtained for that special case, Eq. (91) (cf. [19]).

V. APPLICATIONS TO DIATOMIC MOLECULES N_2 AND O_2

A. Parallel geometry, $\alpha=0$: Elementary expression of $T_e^{(n)}(\theta,\alpha=0)$ for N_2

N_2 has σ_g symmetry, and we approximate its MO by the asymptotic approximation [Eq. (67)] with $m=0$ and $l=0,2,4$ [48,49]. We evaluate Eq. (84) for $m=0$ and $l_i,l_r=0,2,4$ to get the HHG operator for N_2

$$T_e^{(n)}(\theta)=\sqrt{2\pi(n\omega)}\sum_{l_i,l_r=0,2,4}d^{l_r}_{00}(\theta)\tilde{a}^{n}_{zz}(l_r,l_i;0)d^{l_i}_{00}(\theta). \quad (104)$$

Using the expressions for the reduced rotation matrices from Table I and simplifying, we may rewrite the HHG operator as a sum of powers of $\cos^2\theta$ only,

$$T_e^{(n)}(\theta)=\sqrt{2\pi(n\omega)}[b_0^{(n)}+b_1^{(n)}\cos^2\theta+b_2^{(n)}\cos^4\theta+b_3^{(n)}\cos^6\theta+b_4^{(n)}\cos^8\theta], \quad (105)$$

where the coefficients $b_j^{(n)}$'s are

$$b_0^{(n)}=\tilde{a}^{(n)}_{zz}(0,0;0)-\frac{1}{2}\tilde{a}^{(n)}_{zz}(2,2;0)+\frac{3}{8}\tilde{a}^{(n)}_{zz}(4,4;0)-\frac{1}{2}[\tilde{a}^{(n)}_{zz}(0,2;0)+\tilde{a}^{(n)}_{zz}(2,0;0)]+\frac{3}{8}[\tilde{a}^{(n)}_{zz}(0,4;0)+\tilde{a}^{(n)}_{zz}(4,0;0)]$$
$$-\frac{3}{16}[\tilde{a}^{(n)}_{zz}(2,4;0)+\tilde{a}^{(n)}_{zz}(4,2;0)],$$

$$b_1^{(n)}=-\frac{3}{2}\tilde{a}^{(n)}_{zz}(2,2;0)+\frac{3}{2}[\tilde{a}^{(n)}_{zz}(0,2;0)+\tilde{a}^{(n)}_{zz}(2,0;0)]-\frac{15}{4}[\tilde{a}^{(n)}_{zz}(0,4;0)+\tilde{a}^{(n)}_{zz}(4,0;0)]-\frac{21}{16}[\tilde{a}^{(n)}_{zz}(2,4;0)+\tilde{a}^{(n)}_{zz}(4,2;0)],$$

$$b_2^{(n)}=\frac{35}{8}[\tilde{a}^{(n)}_{zz}(0,4;0)+\tilde{a}^{(n)}_{zz}(4,0;0)]-\frac{125}{16}[\tilde{a}^{(n)}_{zz}(2,4;0)+\tilde{a}^{(n)}_{zz}(4,2;0)],$$

$$b_3^{(n)}=\frac{105}{16}[\tilde{a}^{(n)}_{zz}(2,4;0)+\tilde{a}^{(n)}_{zz}(4,2;0)],$$

$$b_4^{(n)}=\frac{1225}{16}\tilde{a}^{(n)}_{zz}(4,4;0). \quad (106)$$

Thus, using Eq. (62), we get the nth harmonic signal for N_2,

$$S^{(n)}(t_d) = \mathcal{C}\sum_{j=0}^{4}\sum_{j'\geqslant j}^{4} c_{jj'}^{(n)}\langle\langle\cos^{2j}\theta\rangle\langle\cos^{2j'}\theta\rangle\rangle$$
$$= \mathcal{C}\{c_{00}^{(n)} + c_{01}^{(n)}\langle\langle\cos^2\theta\rangle\rangle(t_d) + c_{11}^{(n)}\langle\langle\cos^2\theta\rangle^2\rangle(t_d)$$
$$+ c_{02}^{(n)}\langle\langle\cos^4\theta\rangle\rangle(t_d) + \cdots + c_{44}^{(n)}\langle\langle\cos^8\theta\rangle^2\rangle(t_d)\}, \quad (107)$$

where $\mathcal{C}=(\sqrt{2\pi n\omega})^2 2\pi\frac{(n\omega)^2}{c^3}=(2\pi)^2(\frac{n\omega}{c})^3$. The coefficients $c_{jj'}^{(n)}$ are related to $b_j^{(n)}$ as follows:

$$c_{j,j'}^{(n)} = \begin{cases} |b_j^{(n)}|^2 & \text{for } j=j' \\ 2\,\mathrm{Re}(b_j^{(n)}b_{j'}^{(n)*}) & \text{for } j\neq j'. \end{cases} \quad (108)$$

The leading two terms of the signal for N_2, Eq. (107), consist of a constant term proportional to $c_{00}^{(n)}$, which arises from the lowest angular momentum term $l=0$ of the active molecular orbital of N_2, and a term proportional to the second moment $\langle\langle\cos^2\theta\rangle\rangle(t_d)$ that corresponds to the usual "degree of alignment" $A(t_d)$. We may note in passing that the above result does not support a recent model calculation [53,54] that emphasizes that the leading contribution for the HHG signal from N_2 arises from the fourth moment $\langle\cos^4\theta\rangle$; that would require, for example, dropping the basic contribution of the $l=0$ term, i.e., $b_0^{(n)}$ in Eq. (105) of the HHG operator for N_2—which of course could not be justified due to the σ-symmetry of its active orbital.

B. Parallel geometry, $\alpha=0$: Elementary expression of $T_e^{(n)}(\theta;\alpha=0)$ for O_2

O_2 has π_g symmetry, and thus we approximate its MO by the asymptotic approximation with $m=1$ and $l=2,4$ [48,49]. The HHG operator [Eq. (84)] for O_2 reads

$$T_e^{(n)}(\theta) = \sqrt{2\pi(n\omega)}\times\sum_{l_i,l_r=2,4} d_{01}^{l_r}(\theta)\tilde{a}_{zz}^{(n)}(l_r,l_i;1)d_{01}^{l_i}(\theta). \quad (109)$$

By using the expressions for the reduced rotation matrices from Tabel (1) and simplifying, we may rewrite the HHG operator for O_2 as a sum of powers of $\sin^2\theta\cos^{2n}\theta$ only,

$$T_e^{(n)}(\theta) = \sqrt{2\pi(n\omega)}(b_1^{(n)}\sin^2\theta\cos^2\theta + b_2^{(n)}\sin^2\theta\cos^4\theta$$
$$+ b_3^{(n)}\sin^2\theta\cos^6\theta), \quad (110)$$

where $b_j^{(n)}$ coefficients are given by

$$b_1^{(n)} = \frac{3}{2}\tilde{a}_{zz}^{(n)}(2,2;1) + \frac{45}{16}\tilde{a}_{zz}^{(n)}(4,4;1)$$
$$- \frac{3}{4}\sqrt{\frac{15}{2}}[\tilde{a}_{zz}^{(n)}(2,4;1) + \tilde{a}^{(n)}(4,2;1)],$$

$$b_2^{(n)} = -\frac{105}{8}\tilde{a}_{zz}^{(n)}(4,4;1) + \frac{7}{4}\sqrt{\frac{15}{2}}[\tilde{a}_{zz}^{(n)}(2,4;1) + \tilde{a}_{zz}^{(n)}(4,2;1)],$$

$$b_3^{(n)} = \frac{245}{16}\tilde{a}_{zz}^{(n)}(4,4;1). \quad (111)$$

Finally, substituting operator expression [Eq. (110)] in Eq. (62), we obtain the nth signal of O_2

$$S^{(n)}(t_d) = \mathcal{C}\sum_{j=1}^{3}\sum_{j'\geqslant j}^{3} c_{jj'}^{(n)}\times\langle\langle\sin^2\theta\cos^{2j}\theta\rangle\langle\sin^2\theta\cos^{2j'}\theta\rangle\rangle$$
$$= \mathcal{C}\{c_{11}^{(n)}\langle\langle\sin^2\theta\cos^2\theta\rangle^2\rangle(t_d) + c_{12}^{(n)}\langle\langle\sin^2\theta\cos^2\theta\rangle$$
$$\times\langle\sin^2\theta\cos^4\theta\rangle\rangle(t_d) + \cdots$$
$$+ c_{33}^{(n)}\langle\langle\sin^2\theta\cos^6\theta\rangle^2\rangle(t_d)\}. \quad (112)$$

In the above, the coefficients $c_{jj'}^{(n)}$ are related to the $b_j^{(n)}$ coefficients of Eq. (111) through Eq. (108). We add parenthetically that, unlike in the case of N_2 considered above, now there is no constant leading term in the signal for O_2, Eq. (112). This is a consequence of the π *symmetry* of the active orbital for O_2, which does not permit the lowest $l=0$ angular momentum component for its active orbital.

C. Arbitrary relative polarization angle α: HHG signal

We now consider the signals for N_2 and O_2 in the general case in which the probe and the pump polarizations make an arbitrary angle α between them, as shown in Fig. 3. Unlike the axis orientation angle θ, the pump-probe polarization angle α can be controlled directly in the laboratory and thus can provide a possible control over the HHG signal. To express the signals in terms of the moments of elementary trigonometric functions, also in the general case, we refer to Fig. 3. The direction of the molecular axis is now denoted by (θ',ϕ'). The same expression for the signal as in the case of parallel polarization now holds in terms of the primed angles. The HHG signals Eq. (107) for N_2 and Eq. (112) for O_2 for an arbitrary angle α now can be written for N_2 as

$$S^{(n)}(t_d;\alpha) = \mathcal{C}\{c_{00}^{(n)} + c_{01}^{(n)}\langle\langle\cos^2\theta'\rangle\rangle(t_d) + c_{11}^{(n)}\langle\langle\cos^2\theta'\rangle^2\rangle(t_d)$$
$$+ \cdots + c_{44}^{(n)}\langle\langle\cos^8\theta'\rangle^2\rangle(t_d)\} \quad (113)$$

and for O_2 as

$$S^{(n)}(t_d;\alpha) = \mathcal{C}\{c_{11}^{(n)}\langle\langle\sin^2\theta'\cos^2\theta'\rangle^2\rangle(t_d)$$
$$+ c_{12}^{(n)}\langle\langle\sin^2\theta'\cos^2\theta'\rangle\langle\sin^2\theta'\cos^4\theta'\rangle\rangle(t_d)$$
$$+ \cdots + c_{33}^{(n)}\langle\langle\sin^2\theta'\cos^6\theta'\rangle^2\rangle(t_d)\}. \quad (114)$$

Above, we have used the notation $\langle\langle f(\theta')\rangle\rangle(t_d) = \Sigma_{J_0M_0}\rho(J_0)\langle\Phi_{J_0M_0}(t_d,\theta)|f(\theta')|\Phi_{J_0M_0}(t_d,\theta)\rangle$ for the expectation value of a function $f(\theta')$ given in the probe frame, but evaluated with respect to the rotational wave packets defined in the pump frame. Before evaluating the above integral, it is convenient, therefore, to transform the HHG operators from the variables (θ',ϕ') to the angles (θ,ϕ) in the pump-frame (i.e., with the z along the pump polarization). This can be done by the simple transformation Eq. (92), where ϕ is the angle between the plane containing the molecular axis and the pump polarization and the plane containing the pump and the probe polarization directions. Thus, for example, the el-

ementary expression for the expectation value of the alignment operator $A(t_d;\alpha)=\langle\cos^2\theta'\rangle$ in the case of any α reads

$$A(t_d;\alpha)=\langle\cos^2\theta'\rangle=\left(\cos^2\alpha-\frac{1}{2}\sin^2\theta\right)\langle\cos^2\theta\rangle+\frac{1}{2}\sin^2\alpha+\frac{1}{4}\sin^2\alpha(\langle\sin^2\theta e^{2i\phi}\rangle+\text{c.c.})+\frac{1}{2}\sin 2\alpha(\langle\sin\theta\cos\theta e^{i\phi}\rangle+\text{c.c.}),\quad(115)$$

where $\langle\sin\theta\cos\theta e^{\pm i\phi}\rangle$ couples the J' states with $\Delta J=0,\pm 2$ and $\Delta M=\pm 1$, whereas $\langle\sin^2\theta e^{\pm 2i\phi}\rangle$ couples the J' states with $\Delta J=0,\pm 2$ and $\Delta M=\pm 2$. We note that for the linearly polarized pump pulse of the present interest, the interaction Hamiltonian is proportional to $\cos^2\theta$, which is independent of M in the space fixed pump-frame. Thus the M-quantum number of the rotational wave packet remains constant, or $M=M_0$, throughout the evolution. Hence, the expectation values of $\langle\sin\theta\cos\theta e^{\pm i\phi}\rangle$ and $\langle\sin^2\theta e^{\pm 2i\phi}\rangle$ vanish and we get

$$\langle\cos^2\theta'\rangle=\frac{1}{2}(3\cos^2\alpha-1)\langle\cos^2\theta\rangle+\frac{1}{2}\sin^2\alpha.\quad(116)$$

In a similar way, we obtain the expectation value for the higher-order moment

$$\langle\cos^4\theta'\rangle=\frac{1}{8}(35\cos^4\alpha-30\cos^2\alpha+3)\langle\cos^4\theta\rangle+\frac{3}{8}(-10\cos^4\alpha+12\cos^2\alpha-2)\langle\cos^2\theta\rangle+\frac{3}{8}\sin^4\alpha.\quad(117)$$

We note in passing that for $\alpha=0$, $\langle\cos^2\theta'\rangle$ in Eq. (116) and $\langle\cos^4\theta'\rangle$ in Eq. (117) reduce to $\langle\cos^2\theta\rangle$ and $\langle\cos^4\theta\rangle$, respectively.

Thermal averaging Eq. (116) gives us the "degree of alignment" or the alignment moment,

$$A(t_d,\alpha)=\frac{1}{2}(3\cos^2\alpha-1)\langle\langle\cos^2\theta\rangle\rangle(t_d)+\frac{1}{2}\sin^2\alpha,\quad(118)$$

which also appears in the second leading term of the signal for N_2, for arbitrary angle α [see Eq. (113)]. Squaring and taking the thermal average of Eq. (116) gives us $\langle\langle\cos^2\theta'\rangle^2\rangle$, which is the third term of the HHG signal of N_2. The thermal average of Eq. (117) gives us $\langle\langle\cos^4\theta'\rangle\rangle$, which appears in the fourth term of the HHG signal of N_2. The difference of Eqs. (116) and (117) gives us

$$\langle\sin^2\theta'\cos^2\theta'\rangle=\frac{1}{8}(-35\cos^4\alpha+30\cos^2\alpha-3)\langle\cos^4\theta\rangle+\frac{1}{8}(30\cos^4\alpha-24\cos^2\alpha+2)\langle\cos^2\theta\rangle+\frac{1}{8}(-3\sin^4\alpha+4\sin^2\alpha).\quad(119)$$

Squaring and then thermally averaging Eq. (119) yields the leading term of the HHG signal of O_2, given by Eq. (114). In a similar way, we can explicitly exhibit the α dependence of the higher-order terms in the signal for O_2, Eq. (114), as well.

VI. RESULTS AND DISCUSSIONS

A. Signals in the time domain

We now apply the theory to analyze the observed HHG signals from the diatomic molecules, N_2 and O_2. In typical recent experiments (e.g., [11–13]), an ensemble of N_2 or O_2 molecules is first set into free rotation by a femtosecond pump pulse. The HHG signals were detected by monitoring the emission due to a second more intense femtosecond probe pulse, that was delayed with respect to the first by successively increasing the time intervals, t_d, in the picosecond domain, between them.

In the experiments for N_2, for example [13], a peak pump intensity $I_1=0.8\times10^{14}$ W/cm^2 and a peak probe intensity $I_2=1.7\times10^{14}$ W/cm^2 were used; the central wavelength $\lambda=800$ nm and the pulse duration $\tau=40$ fs were kept the same for both the pulses. For the experiment with O_2, the harmonic signal was measured in a similar fashion for $I_1=0.5\times10^{14}$ W/cm^2 and $I_2=1.2\times10^{14}$ W/cm^2; the other parameters were kept the same as in the case of N_2. For the purpose of a direct comparison, our calculations were performed for the same parameter values as in these experiments [13]. In Fig. 4, we show the calculated HHG signals as a function of t_d for N_2 and O_2, obtained for the 19th- and 21st-order harmonic, calculated by using the same parameters as those in the above experiments. The effective ensemble temperature was taken to be $T=200$ K in panels (a) and (c), which was estimated from the matching of the peak position of the spectral distribution with that of the Boltzmann distribution as suggested first in [19]. It can be seen from Fig. 4 [panels (a) and (b)] that the calculated data for N_2 show the "revival" phenomenon with a full revival period $T_{\text{rev}}=8.4$ ps [which is consistent with the rotational constant of N_2 (cf. Table II)] as well as a $\frac{1}{2}$ and a $\frac{1}{4}$ fractional-revival. The calculated signal for O_2 [panels (c) and (d)] shows, in addition to the full revival (period for O_2 is $T_{\text{rev}}=11.6$ ps) and two fractional revivals similar to the two seen for N_2, an additional $\frac{1}{8}$ revival. The calculated signals can be seen to follow the same sequence of the full and the three fractional revivals as seen in the experimental signal [13]. We note that these observations for N_2 and O_2 are also consistent with the data of Itatani *et al.* [11] and Kanai *et al.* [12].

To understand the similarities and the differences between the signals for N_2 and O_2, we use the analytical results of the

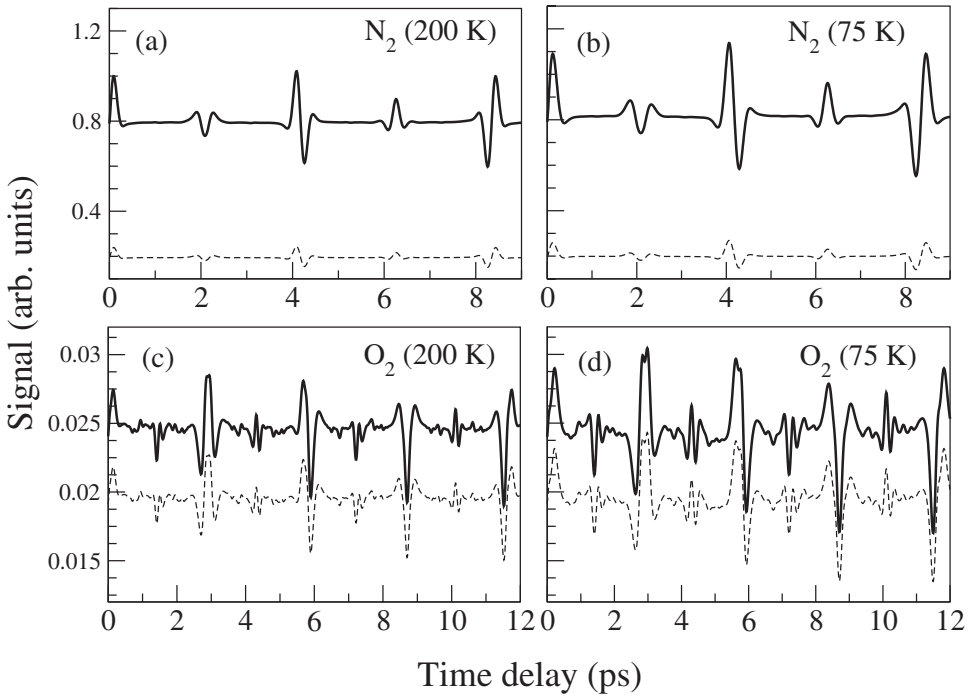

FIG. 4. The calculated dynamic 19th (solid lines) and 21st (dashed lines) HHG signals for N_2 and O_2, for two different initial temperatures, 200 and 75 K. We use pump intensity $I=0.8\times10^{14}$ W/cm^2 for N_2 and $I=0.5\times10^{14}$ W/cm^2 for O_2, probe intensity $I=1.7\times10^{14}$ W/cm^2 for N_2 and $I=1.2\times10^{14}$ W/cm^2 for O_2; duration 40 fs, and wavelength 800 nm.

present theory below. The properties of the HHG signal of N_2 are governed by Eq. (107). The first term gives a constant background. The second term $\langle\langle\cos^2\theta\rangle\rangle(t_d)$ is the dominant dynamic term and causes the signal to mimic the "degree of alignment" $A(t_d)\equiv\langle\langle\cos^2\theta\rangle\rangle(t_d)$. The third term $\langle\langle\cos^2\theta\rangle^2\rangle(t_d)$ give unequal maxima and minima, i.e., the difference between the maximum signal and the average signal is greater than the difference between the average signal and the minimum signal. Furthermore, we point out that at a lower initial temperature, the valley of $\langle\langle\cos^2\theta\rangle^2\rangle(t_d)$ that occurs, for higher temperatures, at the $\frac{1}{4}T_{\rm rev}$ revival, can *split* into two valleys, due to this term, and thus the third term can strongly affect the HHG spectrum, as can be seen in the experiment by Itatani *et al.* [11,14]. Another earlier puzzle regarding its dynamic signal observed was the failure of the alignment measure $A(t_d)=\langle\langle\cos^2\theta\rangle\rangle(t_d)$ to account for the dynamic HHG signal for O_2, observed by Itatani *et al.* [11]. In fact, Itatani *et al.* found that their data behaved more closely to the expectation value $B(t_d)\equiv\langle\langle\sin^2 2\theta\rangle\rangle(t_d)$. From Eq. (112), it can be seen that indeed the *leading* term of the signal for O_2 is given by $\langle\langle\sin^2\theta\cos^2\theta\rangle^2\rangle(t_d)=\frac{1}{16}\langle\langle\sin^2 2\theta\rangle^2\rangle(t_d)$, which is directly proportional to the observed signal. Moreover, the present theory also predicts that there ought to be modifications to this result due to the higher-order terms in Eq. (112). In fact, as mentioned earlier, Kanai *et al.* [12] found empirically that their experimental HHG signals for N_2 and O_2 demanded heuristic introduction of operators involving *higher* orders of $\cos^2\theta$ functions, or Legendre polynomials, as the dynamic signal could not be well expressed in term of $\langle\langle\cos^2\theta\rangle\rangle(t_d)$ only for N_2, or $\langle\langle\sin^2 2\theta\rangle\rangle(t_d)$ only for O_2. They can be, however, quantitative contributions from the higher-order terms predicted by the theory. In fact, the present theory provides an *ab initio* derivation of the desired general expansion of the HHG signal in terms of the moments of the Legendre polynomials Eq. (103) and/or of the powers of $\cos^2\theta$, e.g., Eqs. (112) and (107).

TABLE II. Molecular properties used in this work: I_p is adiabatic ionization potential, B is rotational constant of molecule, $\alpha_\parallel$ and $\alpha_\perp$ are parallel and perpendicular polarizability, and $C_l^{(m)}$'s are angular coefficient of the electronic wave function.

	N_2	O_2	Ref.
HOMO	σ_g, $m=0$	π_g, $m=1$	[22,50]
I_p (eV)	15.58	12.03	[48]
B (cm^{-1})	2.0	1.4377	[51]
$\alpha_\parallel$ (Å^3)	2.38	2.35	[52]
$\alpha_\perp$ (Å^3)	1.45	1.21	[52]
$C_0^{(m)}$	2.02		[48]
$C_2^{(m)}$	0.78	0.62	[48]
$C_4^{(m)}$	0.04	0.03	[48]

A related characteristic of interest is the appearance of extra series and lines (e.g., [13,19]) in the Fourier spectrum of the dynamic HHG signal for *both* N_2 and O_2, which are Raman forbidden. These extra lines cannot be attributed to $A(t_d)=\langle\langle\cos^2\theta\rangle\rangle(t_d)$ for N_2, or to $B(t_d)=\langle\langle\sin^2 2\theta\rangle\rangle(t_d)$ for O_2. It will be seen below that the FT of the higher-orders terms of Eq. (107) for N_2 and of Eq. (112) for O_2, given by the present theory, can consistently account for their appearance. Comparing the expressions for the signals for N_2 and O_2 and directly calculating the $c_{jj'}^{(n)}$ coefficients in the respec-

tive signals, it is found that the signal for N_2 is much stronger than that for O_2.

We may briefly discuss here the dependency of the HHG signals on the initial temperature, an example of which is shown in Fig. 4. It can be seen from the figure that the lower initial temperature gives a greater amplitude of revival. This may be understood as follows. A lower initial temperature gives a lower value of the maximum of the statistically occupied J_0 levels and hence also a lower value of the maximum initial value of M_0 than at a higher temperature. As a result of interaction with the linearly polarized pump pulse (quantization axis along the polarization axis) at a given intensity, each wave packet that evolves from a given initial $|J_0M_0\rangle$ state can couple to the higher levels $J' > \max(J_0)$ but cannot raise the initial maximum value of M_0. Therefore, for a given intensity, the ratio of J' to M_0 is higher for a lower temperature, and as a consequence the degree of alignment $A(t_d)=\langle\langle\cos^2\theta\rangle\rangle$ tends to be also higher, implying that the molecule becomes more strongly aligned during a revival.

B. Rotational revivals: Periods and phases

If a linear molecule has a permanent dipole moment (e.g., heteronuclear diatomics), then the interaction Hamiltonian of the (pump) laser with the molecular frame depends on the first power of $\cos\theta$, where θ is the angle of rotation of the molecular axis with respect to the laser polarization axis. In contrast, the interaction with the polarizability of the molecule (e.g., for homo- or heteronuclear diatomics) depends on $\cos^2\theta$. Thus in general the interaction may contain the operators $\cos^n\theta$ with $n=1$ and/or 2. Then in either case, the rotational wave packets created by the latter can be written in the form

$$\Phi_{J_0M_0}(t) = \sum_{j=0,1,2,3,\ldots} C_{J_0+nj,M_0}(t) \times e^{-i/\hbar E_{J_0+nj}t}|J_0+nj,M_0\rangle. \tag{120}$$

This can be obtained, for example, from a consideration of the perturbative solution of Eq. (39) in successive power of the interaction Hamiltonian, and noting that the rotational eigenstates couple either by $P_2(\cos\theta)$ (in the absence of a permanent dipole moment) with a minimum (nonzero) $n=2$ or by $P_1(\cos\theta)$ and $P_2(\cos\theta)$ (in the presence of a permanent dipole moment) with a minimum $n=1$. It can be readily understood from the well known properties of the vector addition coefficients that appear in the integration over the product of three spherical harmonics (cf. the paragraph below) that the expectation value of the Nth cosine-moment with respect to a rotational wave packet at a time $t=t_d$ takes the form

$$\begin{aligned}\langle\cos^N\theta\rangle_{J_0M_0}(t_d) &= \langle\Phi_{J_0M_0}(t_d)|\cos^N\theta|\Phi_{J_0M_0}(t_d)\rangle \\ &= \sum_s^N \sum_{p=-s}^{s} \sum_{j=0,1,2,3,\ldots} \times C^{J_0M_0*}_{J_0+nj+p,M_0}(t_d) \\ &\quad \times C^{J_0M_0}_{J_0+nj,M_0}(t_d) \\ &\quad \times a_s\langle Y_{J_0+nj+p,M_0}|Y_{s,0}|Y_{J_0+nj,M_0}\rangle \\ &\quad \times \exp\left(-\frac{i}{\hbar}(E_{J_0+nj+p}-E_{J_0+nj})t_d\right),\end{aligned} \tag{121}$$

where the integers s and p have the same parity (even or odd) as the parity of N. This follows from the fact that $\cos^N\theta$ can be expressed as a linear combination: $\cos^N\theta = \Sigma_s a_s P_s(\cos\theta)$ for all s up to N, and since the matrix elements $\langle Y_{J_0+nj',M_0}|Y_{s,0}|Y_{J_0+nj,M_0}\rangle = 0$, unless $J_0+nj' = J_0+nj+(p-s) \geq 0$ and $J_0+nj+(p-s)+J_0+nj+s=$even. Thus, the phase of each individual term of Eq. (121), for any given value of the integers J_0, n, N, j, is given by

$$\begin{aligned}\Delta\phi^{J_0}_{n,N}(t_d) &= \frac{1}{\hbar}(E_{J_0+nj+p}-E_{J_0+nj})t_d \\ &\quad \times 2\pi hBct(\pm 2pJ_0 \pm 2npj + p^2 \pm p) \\ &= 2\pi\frac{t_d(hBc)2}{\hbar}\left(J_0+nj+\frac{p^2+p}{2}\right),\end{aligned} \tag{122}$$

where we have used $E_{J,M} \equiv J(J+1)hBc$; B is the rotational constant, $T_{\rm rev} \equiv \frac{1}{2Bc}$ is the rotational period, and $h=2\pi\hbar$. We note first that the quantity in the last set of parentheses above is an integer, independent of the value of j and J_0. We note that the maximum value of s or p above is N. The phase difference [Eq. (122)], therefore, equals an even or odd multiple of π, or an odd multiple of $\frac{\pi}{2}$, depending on the parity of the groups of rotational states. Therefore, the shortest time period for which the phases of *all* terms or all terms within a parity group become equal in Eq. (122), and hence coherently enhance the signal, is clearly

$$T_{\rm min} = \frac{1}{nN}T_r. \tag{123}$$

For times between the successive coherent enhancements or "revivals," the individual phases in Eq. (122) disperse away from one another and the revival peaks tend to be washed out by destructive interference, and the HHG signal reduces to the average or the background level.

We may summarize the above result as a "revival theorem": If the laser-molecule interaction Hamiltonian is characterized by the lowest power n of $\cos^n\theta$, with $n=1$ or 2, θ is the rotation angle, and if the highest discernible (numerically significant) moment in the expression of the signal is $\langle\Phi_{J_0M_0}(t)|\cos^N\theta|\Phi_{J_0M_0}(t)\rangle$, $N \geq 1$, then the experimental signal would exhibit as many as $n\times N$ revivals within a full period $T_r = \frac{1}{2Bc}$, where B is the rotational constant. Inversely, by counting the number of fractional revivals in the observed HHG signal, one may determine the highest order, N, and hence also the significant "cosine moments" (up to the order N) that would be necessary to fit the observed signal. We may note that the above theorem covers the well-known cases of fractional revivals discussed earlier [55–58] as special cases.

For homonuclear diatomic molecules with no permanent dipole moment, the lowest order pump pulse interaction is due to the polarizability tensor with $n=2$. Thus for the standard alignment moment, $A(t_d) \equiv \langle\langle\cos^2\theta\rangle\rangle(t_d)$ with $N=2$, we

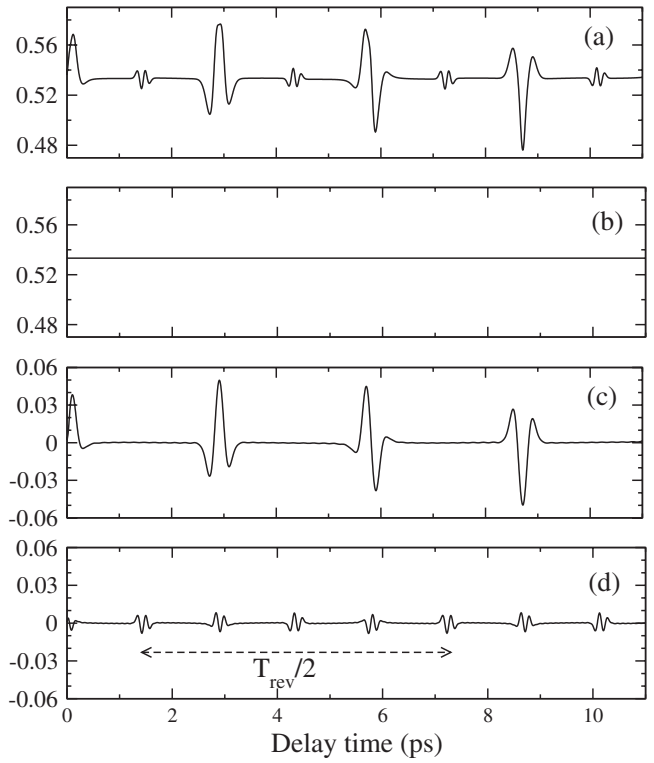

FIG. 5. Revival structure of the moment $\langle\langle \sin^2 2\theta\rangle\rangle(t_d)$, for the case of O_2, on the beat frequency: for all ΔJ retained (panel a), with $\Delta J=0$ only (panel b), with $\Delta J=\pm 2$ only (panel c), and with $\Delta J=\pm 4$ only (panel d). It is clear that the transition with $\Delta J=\pm 4$ has the lowest fractional revival at $\frac{1}{8}T_{\rm rev}$, and has the shortest period.

get the lowest fractional period $T_{1/4}=\frac{1}{4}T_r$, and the subsequent two fractional revivals $T_{1/2}$, $T_{3/4}$ (defined analogously) and the full revival at T_r, within a period. Thus the presence of the highest significant fourth cosine-moment with $N=4$ would show the lowest $\frac{1}{nN}=\frac{1}{8}$ revival, plus the subsequent six fractional revivals at $(\frac{1}{4},\frac{3}{8},\frac{1}{2},\frac{5}{8},\frac{3}{4},\frac{7}{8})$ T_r, within a full period T_r. An example containing the effect of the fourth cosine-moment is $B(t_d)=\langle\langle \sin^2 2\theta\rangle\rangle(t_d)$, which is illustrated in Fig. 5. For a heteromolecular diatomic molecule with a permanent dipole moment, the lowest-order interaction Hamiltonian is characterized by the first power of cos θ, i.e., $n=1$. Thus the alignment measure, a cosine moment with $N=2$, will show $n\times N=2$ revivals within the full period. Higher-order revivals may occur since Eq. (123) in principle holds for any combination (N,n). We may recall, however, that for large N, the expectation value might be too weak for the lowest fractional revivals to be measured with sufficient resolution in practice. This circumstance is illustrated in Fig. 6, which shows the high-order fractional revivals for $N=6$ and 8 cosine moments, $\langle\langle \cos^6\theta\rangle\rangle(t_d)$ and $\langle\langle \cos^8\theta\rangle\rangle(t_d)$, along with their magnifications.

C. Phase relations of fractional revivals

Can one predict the relative phases of the fractional revivals? We may answer this question positively. From the phase difference [Eq. (122)], one finds

$$\Delta\phi_{2,2}^{J_0+1}(T_{\rm rev})-\Delta\phi_{2,2}^{J_0}(T_{\rm rev})=4\pi,$$

$$\Delta\phi_{2,2}^{J_0+1}(T_{\rm rev}/2)-\Delta\phi_{2,2}^{J_0}(T_{\rm rev}/2)=2\pi,$$

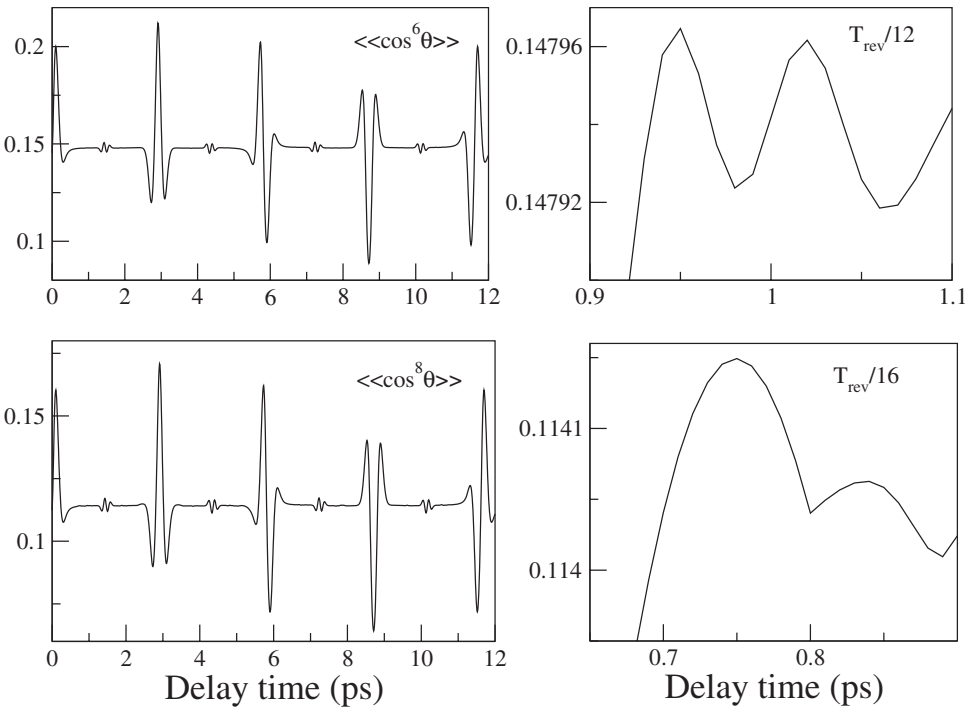

FIG. 6. Weak components of the fractional revivals in the dynamical alignment signal for the case of O_2. Contribution from $\langle\langle \cos^6\theta\rangle\rangle(t_d)$, near $T_{\rm rev}/12$ (upper panel), and from $\langle\langle \cos^8\theta\rangle\rangle(t_d)$, near $T_{\rm rev}/16$ (lower panel). They can hardly be detected in the full delay-time signal that is dominated by the leading lower order moments. $I=0.5\times 10^{14}$ W/cm^2, FWHM 40 fs, and initial temperature 300 K.

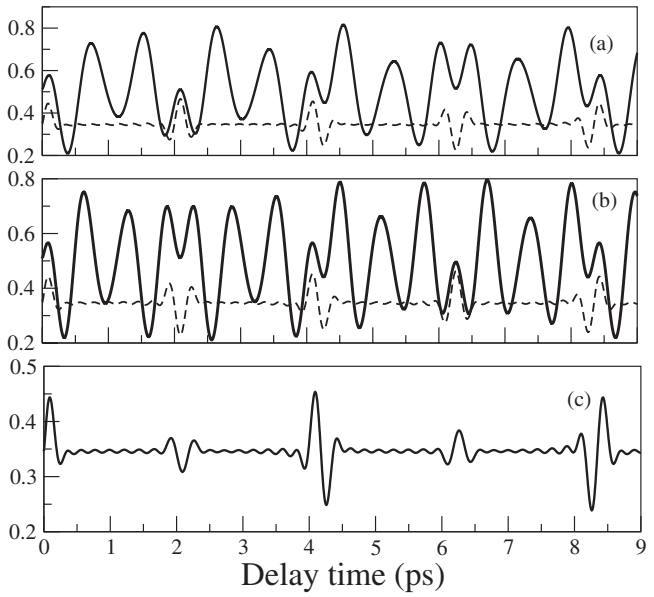

FIG. 7. Dependence of alignment moment $\langle\langle\cos^2\theta\rangle\rangle(t_d)$ (for the case of N_2) on $|J_0,M_0\rangle$. (a) Calculated with a single state $|5,0\rangle$ only (solid line), and retaining all odd J_0 with $J_{max}=19$ (dashed line). (b) With $|6,0\rangle$ only (solid line), and all even J_0 with $J_{max}=20$ (dashed line). (c) Calculated with all J up to $J_{max}=20$. Results are for pulse intensity 0.8×10^{14} W/cm^2 and with FWHM 40 fs, for initial temperature 300 K.

$$\Delta\phi_{2,2}^{J_0+1}(T_{rev}/4)-\Delta\phi_{2,2}^{J_0}(T_{rev}/4)=\pi. \tag{124}$$

Equation (124) predicts that at $\frac{1}{4}T_r$ the phase for J_{even} is an exact mirror image of the phase for J_{odd}, as in fact is the case in Fig. 7, calculated for N_2. From the above, we may further predict that (a) O_2, which possesses J_{odd} levels only, will show a "peak" at $T_r/4$, (b) CO_2, which possesses J_{even} levels only, will show a "valley" at $T_r/4$, and (c) N_2, which possesses both the majority J_{even} levels and the minority J_{odd} levels in the ratio 2:1 (due to the nuclear statistics of the molecule [22]), will show the revival at $T_r/4$ that would be a "valley" like the one for the J_{even} levels only, but with only half its normal "depth," due to the counter contribution from the minority J_{odd} levels.

We note that one may also predict the nuclear statistics of such molecules by comparing the revival shape at $T_{rev}/2$ and $T_{rev}/4$. Let us first define a modulation amplitude at half-revival to be equal to the difference between peak and the base (or average) signal: $(A_{1/2}=S_{1/2}^{top}-S_{1/2}^{av})$. Similarly, a modulation amplitude at quarter revival is equal to the difference between the top and the base (average) signal: $(A_{1/4}=S_{1/4}^{top}-S_{1/4}^{av})$. The amplitude at half-revival is a sum of even and odd J contributions, and therefore $A_{1/2}$ is always positive. In contrast, the amplitude at the quarter-revival arises from their difference, and therefore $A_{1/4}$ can be positive (if it makes a "top" alignment) or negative (if it makes an "antitop" alignment). Therefore, the existence of a "top" signal at the quarter-revival is a sign that even J levels are dominant. Similarly the presence of an "antitop" signal at the quarter-revival signal is a sign of dominant odd J levels. From this observation, one can deduce the nuclear statistics

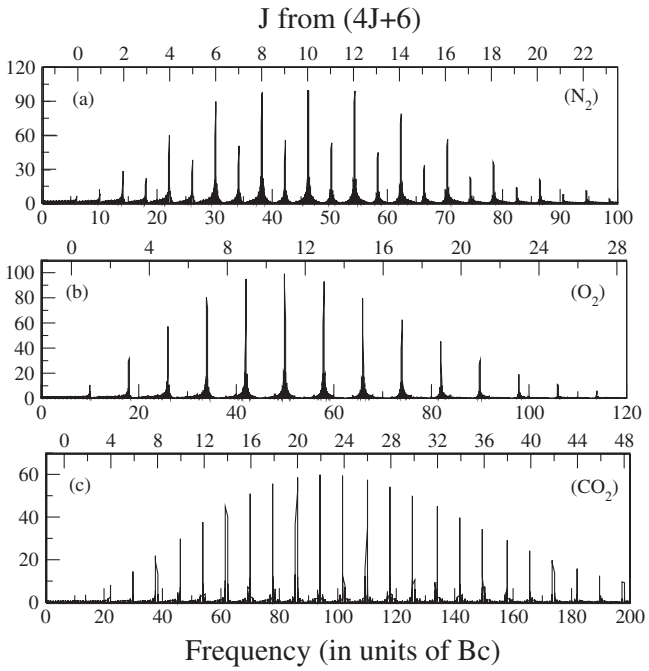

FIG. 8. Fourier transform of the alignment moment $A(t_d)\equiv\langle\langle\cos^2\theta\rangle\rangle(t_d)$, plotted using Bc as the basis frequency (lower scale). Following the $(4J+6)$ rule for the line positions from $\langle\langle\cos^2\theta\rangle\rangle$, the peak frequencies are seen to occur for odd J only for the case of O_2, even J only for the case of CO_2, and for both even and odd J for the case of N_2. The corresponding J values are shown in upper scale.

from the ratio between the effective (finite) number of even and odd J levels (J_{even} and J_{odd}, respectively) excited,

$$\frac{J_{even}}{J_{odd}}=\frac{A_{1/2}-A_{1/4}}{A_{1/2}+A_{1/4}}. \tag{125}$$

Thus, for example, the dynamic signal of O_2 shows $A_{1/2}=A_{1/4}$ indicating the absence of the even J levels. In contrast, $A_{1/2}=-A_{1/4}$ for CO_2, indicating the absence of odd J levels. For N_2, we have $A_{1/4}=-\frac{1}{3}A_{1/2}$, and hence we have $J_{even}:J_{odd}=2:1$. This property might be used for detecting the existence of isotopes of a molecular sample, as has been suggested recently [59].

D. Beat frequencies

From Eq. (121), it is seen that the phase difference associated with $\langle\cos^2\theta\rangle$ is $(B/\hbar)(4J+6)$. For B in cm^{-1}, the phase difference reads

$$\Delta\phi(J\to J\pm2)=2\pi Bc(4J+6) \tag{126}$$

with c in cm/s. According to Eq. (126), one can make a Fourier transform of $\langle\cos^2\theta\rangle$ using Bc as basis frequency and find a series of peaks at $(4J+6)$. Figure 8 shows the Fourier transform of $\langle\langle\cos^2\theta\rangle\rangle$ of N_2, O_2, and CO_2. The spectrum of O_2 has peak series at $(10,18,26,\ldots)Bc=(4J_{odd}+6)Bc$, showing that O_2 has odd J levels only. In contrast, the peak series of CO_2 are located at $(6,14,22,30,\ldots)Bc=(4J_{even}+6)$, showing that CO_2 has even J levels only. For N_2, we

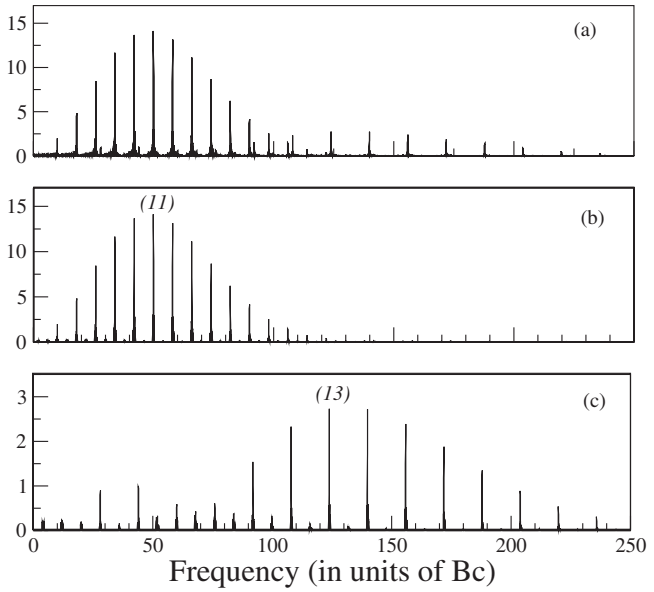

FIG. 9. Fourier transform of $\langle\langle \sin^2 2\theta\rangle\rangle$ of O_2: all lines (panel a), line from transitions with $\Delta J=\pm 2$ only (panel b), and lines from transition with $\Delta J=\pm 4$ only (panel c); pulse of intensity 0.5×10^{14} W/cm^2, FWHM=40 fs, initial temperature 300 K.

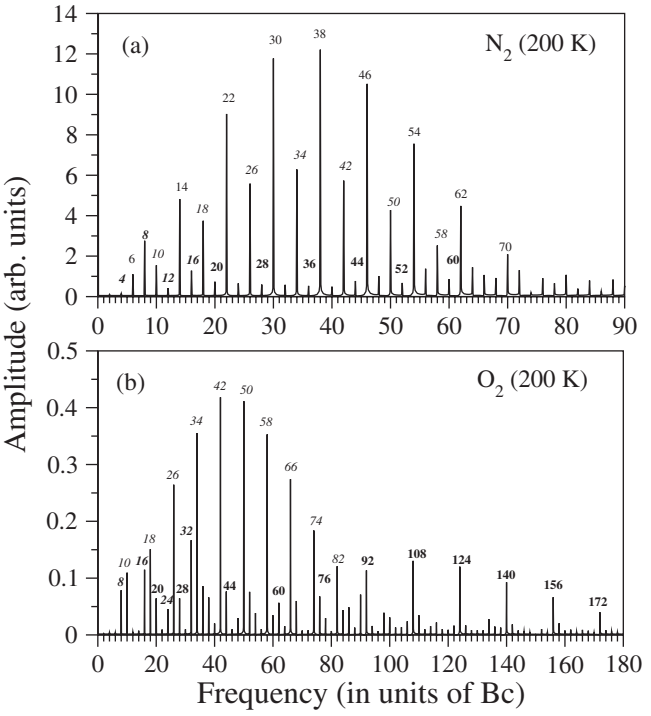

FIG. 10. The theoretical Fourier spectrum for the dynamic 19th harmonic signal for N_2 (panel a) and O_2 (panel b), which are the Fourier spectra of Figs. 4(a) and 4(c), respectively. The spectra of N_2 show series I: $(6,14,22,30,38,\ldots)Bc$, series II: $(10,18,26,34,42,\ldots)Bc$, series III: $(\mathbf{20},\mathbf{28},\mathbf{36},\mathbf{44},\mathbf{52},\ldots)Bc$, and series IV: $(\boldsymbol{4},\boldsymbol{8},\boldsymbol{12},\boldsymbol{16},\ldots)Bc$. The spectra of O_2 show series II, series III, and series V: $(\boldsymbol{8},\boldsymbol{16},\boldsymbol{24},\ldots)Bc$. Please refer to [19] for a direct comparison with the experimental data.

obtain a series $(6,14,22,30,\ldots)Bc=(4J_{\text{even}}+6)$ that is twice as strong as the series $(10,18,26,\ldots)Bc=(4J_{\text{odd}}+6)Bc$. It implies that both even and odd J levels are present in N_2, in the ratio $J_{\text{even}}:J_{\text{odd}}=2:1$. These conclusions are consistent with the analysis based on the dynamic signals.

For $\langle\langle \sin^2 2\theta\rangle\rangle$, there are two kinds of difference or beat frequency. The first one is related to the transitions with $\Delta J=\pm 2$ and is expressed by Eq. (126). The second one is related to the transitions with $\Delta J=\pm 4$ and can be expressed as

$$\Delta\phi(J\rightarrow J\pm 4)=2\pi Bc(8J+20). \tag{127}$$

As a result, in addition to the series of lines $(4J+6)$, the Fourier transform of $\langle\langle \sin^2 2\theta\rangle\rangle$ also has another series of lines at $(8J+20)$, with $\Delta J=4$. Figure 9 shows the calculated Fourier transform of $\langle\langle \sin^2 2\theta\rangle\rangle$ of O_2. It is seen from Fig. 9 that the first series $(\Delta J=\pm 2)$ reaches its maximum at $J_{\max}=11$, while the second one $(\Delta J=\pm 4)$ at $J_{\max}=13$. This difference comes from the fact that the $\Delta J=4$ transition requires $\Delta J=2$ as an intermediate transition. As a result, a $\Delta J=4$ transition can occur one step after the $\Delta J=2$ transition; for O_2 with only J_{odd} levels present, this implies a shift in J by 2, from $J_{\max}=11$ to $J_{\max}=13$, as seen above. From Fig. 9, one also finds that the intensity of the second transition is smaller than that of the first one. This arises from the circumstance that the allowed matrix element of the second transition with the greater separation in J is weaker than the one with the lesser separation.

E. Signals in the frequency domain

To further compare with experimental data, we Fourier transform the calculated dynamic signals to get their spectra in the frequency domain. They may then be compared with the FT. of the experimental data. The results for the 19th harmonic signal for N_2 are shown in Fig. 10(a). It can be seen that the theoretical spectrum exhibits two prominent series I: $(6,14,22,30,\ldots)Bc$ and II: $(10,18,26,34,\ldots)Bc$, which are also present in the experimental spectrum [19]. They can be easily understood to arise from the FT of the $\langle\langle \cos^2\theta\rangle\rangle(t_d)$ term in Eq. (107), which vanishes unless $\Delta J=0,\pm 2$; this produces a sequence of lines $(E_{J+2}-E_J)/2\pi=(4J+6)Bc$, and gives the series I and II for the even and the odd J levels, respectively. The relative prominence of the series I over the series II, from both experiment and theory, seen in Fig. 10(a), could be understood as the 2:1 ratio of the J even over J odd levels, a well-known consequence of the nuclear spin statistics of N_2 (e.g., [8,22]).

The weakly resolved series III: $(\mathbf{20},\mathbf{28},\mathbf{36},\mathbf{44},\ldots)Bc$ and series IV: $(\boldsymbol{4},\boldsymbol{8},\boldsymbol{12},\boldsymbol{16},\ldots)Bc$ in Fig. 10(a) are the unexpected series that could not be produced by the FT of the leading term $\langle\langle \cos^2\theta\rangle\rangle(t_d)$. To interpret their origin, we consider the two higher-order terms involving $\langle\langle \cos^2\theta\rangle^2\rangle(t_d)$ and $\langle\langle \cos^4\theta\rangle\rangle(t_d)$ in the signal for N_2, Eq. (107). Because of the presence of the square of the second moment, the expected beat frequencies from $\langle\langle \cos^2\theta\rangle^2\rangle(t_d)$ not only include the frequencies $(4J+6)Bc$ but also their sum and difference frequencies, as indicated below,

TABLE III. List of all the predicted series arising from the moments $\langle\langle\cos^2\theta\rangle\rangle$, $\langle\langle\cos^2\theta\rangle^2\rangle$, and $\langle\langle\cos^4\theta\rangle\rangle$ that are present in the expression for the signal for N_2 (for which both odd and even J 's are allowed).

No.	Group freq.	Weighting factor	Formula	Peak series (in units of Bc)	Expt. series
$\langle\langle\cos^2\theta\rangle\rangle$					
1		a		0	
2	ω_1	b	$4J+6$	10,18,26,… for odd J 6,14,22,… for even J	II I
$\langle\langle\cos^2\theta\rangle^2\rangle$					
3		aa'		0	
4	ω_1 and ω_1'	$a'b$ and ab'	$4J+6$	10,18,26,… for odd J 6,14,22,… for even J	II I
5	$\omega_1+\omega_1'$	$\frac{bb'}{2}$	$4(J+J')+12$	20,28,36,…	III
6	$\omega_1-\omega_1'$	$\frac{bb'}{2}$	$4(J-J')>0$	4,8,12,…	IV
$\langle\langle\cos^4\theta\rangle\rangle$					
7		a		0	
8	ω_1	b	$4J+6$	10,18,26,… for odd J 6,14,22,… for even J	II I
9	ω_2	c	$8J+20$	28,44,60…	III

$$(a+b\cos\omega_1 t)(a'+b'\cos\omega_1' t)=aa'+a'b\cos\omega_1 t+ab'\cos\omega_1' t+bb'\cos\omega_1 t\cos\omega_1' t=aa'+a'b\cos\omega_1 t+ab'\cos\omega_1' t+\frac{bb'}{2}\cos(\omega_1+\omega_1')t+\frac{bb'}{2}\cos(\omega_1-\omega_1')t. \tag{128}$$

Above, the term a arises from the transitions with $\Delta J=0$ with $\omega_0=0$. The frequency ω_1 arises from the transitions with $\Delta J=\pm 2$. The sum frequency $(\omega_1+\omega_1')$ yields the $(E_{J+2}-E_J)/2\pi\equiv[4(J+J')+12]Bc$ beats, whereas the difference $(\omega_1-\omega_1')$ produces the beats $(E_{J+2}-E_J)/2\pi\equiv[4(J-J')Bc]>0$. For integer J and J' they yield the series IV: $(\boldsymbol{4},\boldsymbol{8},\boldsymbol{12},\boldsymbol{16},\ldots)Bc$. The next term $\langle\langle\cos^4\theta\rangle\rangle(t_d)$ vanishes, unless $\Delta J=0,\pm 2$ and ± 4, produces not only beats $(E_{J+2}-E_J)/2\pi=(4J+6)Bc$ but also $(E_{J+4}-E_J)/2\pi=(8J+20)Bc$ that generates the series III $(\boldsymbol{20},\boldsymbol{28},\boldsymbol{36},\boldsymbol{44},\ldots)Bc$. All the possible series arising from these three leading terms of the signal, and their grouping according to those observed experimentally, are shown in Table III. Note that series III is identical, and overlaps with series IV: $(\boldsymbol{4},\boldsymbol{8},\boldsymbol{12},\boldsymbol{16},\ldots)Bc$ and adds to its signal strength. Moreover, the remaining lines at $(\boldsymbol{4},\boldsymbol{8},\boldsymbol{12},\boldsymbol{16},\boldsymbol{24},\boldsymbol{32},\ldots)Bc$ found in the experimental spectrum [13], as well as in the theoretical spectrum in Fig. 10(a), confirm the existence of series IV, which only partially overlaps with series III. The existence of series III and IV unambiguously shows that the dynamic signal of N_2 cannot be fully described in terms of $\langle\langle\cos^2\theta\rangle\rangle(t_d)$ only.

In Fig. 10(b), we present the theoretical spectrum calculated from Eq. (112), which agrees well with the experimental one [13]. Both the experimental [13] and the theoretical spectra show the Raman-allowed series II: $(10,18,26,34,42,\ldots)Bc$, but not the series I: $(6,14,22,30,38,\ldots)Bc$, seen for N_2. The anomalous series III: $(\boldsymbol{20},\boldsymbol{28},\boldsymbol{36},\boldsymbol{44},\ldots)Bc$, discussed in the case of N_2 above, however, appears for O_2 as well. Finally, another anomalous sequence V: $(\boldsymbol{8},\boldsymbol{16},\boldsymbol{24},\ldots)Bc$ can be seen to be present in the experimental data for O_2 [13], which, we point out, cannot be generated by the FT of the $\langle\langle\sin^2 2\theta\rangle\rangle$ term. To interpret the origin of the observed series in O_2, we first consider the leading term given by Eq. (109), $\langle\langle\sin^2\theta\cos^2\theta\rangle^2\rangle$. The matrix element $\langle\sin^2\theta\cos^2\theta\rangle$ vanishes unless $\Delta J=0,\pm 2,\pm 4$ corresponds to frequency ω_0, ω_1, and ω_2. Thus, there appears the sum and difference frequencies due to the presence of the squared moments in the signal expression, as follows:

$$(a+b\cos\omega_1 t+c\cos\omega_2 t)(a'+b'\cos\omega_1' t+c'\cos\omega_2' t)=aa'+ab'\cos\omega_1' t+a'b\cos\omega_1 t+ac'\cos\omega_2' t+a'c\cos\omega_2 t+\frac{bb'}{2}\cos(\omega_1+\omega_1')t+\frac{bb'}{2}\cos(\omega_1-\omega_1')t+\frac{cc'}{2}\cos(\omega_2+\omega_2')t+\frac{cc'}{2}\cos(\omega_2-\omega_2')t+\frac{bc'}{2}\cos(\omega_1+\omega_2')t+\frac{bc'}{2}\cos(\omega_1-\omega_2')t+\frac{b'c}{2}\cos(\omega_2+\omega_1')t+\frac{b'c}{2}\cos(\omega_2-\omega_1')t, \tag{129}$$

TABLE IV. All possible frequencies arising from $\langle\langle \sin^2 \cos^2 \theta\rangle^2\rangle$ for O_2, whose only odd J's are allowed. The weak frequencies are indicated with *.

No.	Group freq.	Weighting factor	Formula	Peak series (in units of Bc)	Expt. series
1		aa'		0	
2	ω_1 and ω_1'	$a'b$ and ab'	$4J+6$	10,18,26,…	II
3	ω_2 and ω_2'	$a'c$ and ac'	$8J+20$	28,44,60,…	III
4	$\omega_1+\omega_1'$	$\frac{bb'}{2}$	$4(J+J')+12$	20,28,36,…	III
5	$\omega_1-\omega_1'$	$\frac{bb'}{2}$	$4(J-J')>0$	8,16,24,…	V
6	$\omega_2+\omega_2'$	$\frac{cc'}{2}$	$8(J+J')+40$	56,72,88,…	I*
7	$\omega_2-\omega_2'$	$\frac{cc'}{2}$	$8(J-J')>0$	16,32,48,…	V*
8	$\omega_1+\omega_2'$ and $\omega_2+\omega_1'$	$\frac{bc'}{2}$ and $\frac{b'c}{2}$	$4(J+2J')+26$	38,46,54,…	VI*
9	$\omega_1-\omega_2'$	$\frac{bc'}{2}$	$4(J-2J')-14>0$	6,14,22,…	VI*
10	$\omega_2-\omega_1'$	$\frac{b'c}{2}$	$4(-J+2J')+14>0$	2,10,18,…	II*

where, in general, $a>b>c$. As also found earlier above, the frequency ω_1 generates the lines $(4J+6)$ that, for odd J's, yield the series II: $(10,18,26,\ldots)Bc$. The series I: $(6,14,22,\ldots)Bc$ that would exist for even J's is absent from the O_2 spectrum. This is easily understood as due to the nuclear spin of O atoms, which is 0, that strictly forbids any even J rotational levels for O_2 (as dictated by the overall symmetry of the total wave function for O_2). For odd J, the frequency ω_2 produces the lines $(8J+20)Bc=(28,44,60,\ldots)Bc$, whereas the sum frequency $(\omega_1+\omega_1')$ produces the lines $[4(J+J')+12]Bc=(20,28,36,\ldots)Bc$; taken together, they generate the series III: $(\mathbf{20},\mathbf{28},\mathbf{36},\mathbf{44},\ldots)Bc$. Similarly, the difference frequency $\omega_1-\omega_2$ gives rise to the series V: $(\boldsymbol{8},\boldsymbol{16},\boldsymbol{24},\ldots)Bc$, as shown in Table IV. All the above predicted series are seen in the Fourier spectrum for O_2. It is shown in Table IV that the frequency $\omega_1+\omega_2'$ and $\omega_2+\omega_1'$ produces the weak (strength of order "bc") series VI: $[4(J+2J')+26]Bc=(38,46,54,\ldots)Bc$. Despite its weakness, the existence of this series is evidenced by the presence of the discrete line at 38 Bc. It is also worth noting that the series V and VI cannot be generated from the moment $\langle\langle \sin^2 2\theta\rangle\rangle$ alone. The remaining higher-order terms in Eq. (112) contribute, generally very weakly, either to the lines in the series discussed above or to additional lines that can be seen to be present in Fig. 10(b).

Figure 11 shows a calculated spectrum for initial temperature 75 K whose peaks are shifted from one of 200 K (Fig. 10). Comparing those two figures, we may point out that the relative strengths of the lines in a calculated spectrum were found to depend sensitively on the assumed molecular temperature, which is known to be difficult to determine experimentally. This observed sensitivity suggests a useful means to estimate the temperature of the molecular ensemble of interest in the experiment, by requiring that the strongest rotational line in the Fourier spectrum of the dynamic HHG

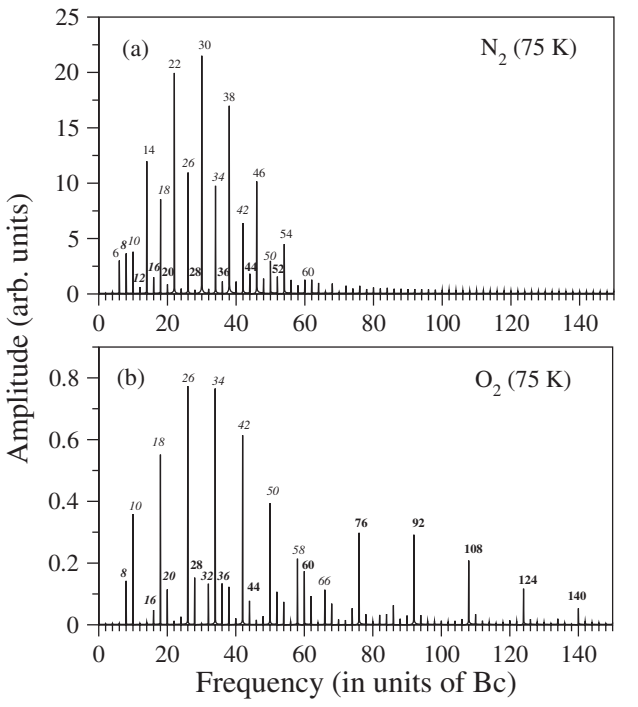

FIG. 11. Calculated spectra for N_2 (panel a) and O_2 (panel b) at a Boltzmann temperature 75 K, which are the Fourier transform of Figs. 4(b) and 4(d), respectively.

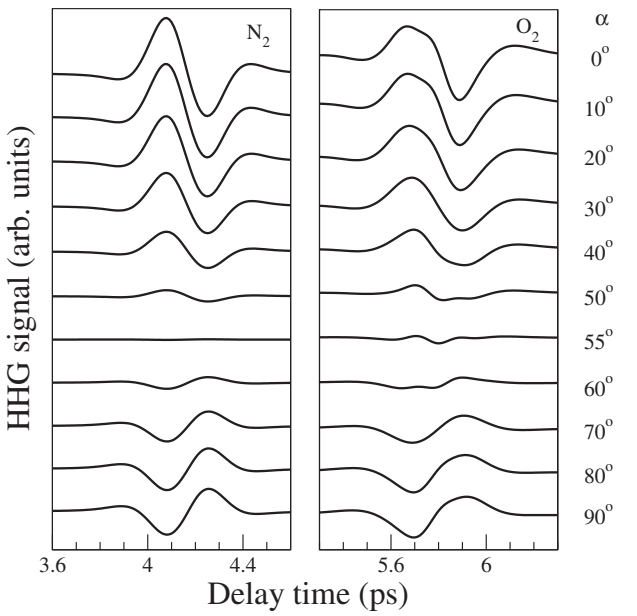

FIG. 12. Calculated 19th harmonic dynamic signal for N_2 (left panel) and O_2 (right panel) for various pump-probe polarization angles. The laser parameters are similar to those in Fig. 4. The initial temperature is 200 K.

signal should correspond to the most highly occupied rotational level in the thermally distributed initial rotational levels. Hence the temperature of the initial Boltzmann distribution may be found by adjusting the temperature to make the level at the peak of the Boltzmann distribution match with the highest line of the Fourier spectrum of the HHG signal observed. Moreover, the spectral information in the frequency domain of the time-domain HHG signal is more succinct because of its discreteness and could be used, for example, to distinguish between various theoretical models (see Sec. VII D).

F. Interplay of polarization geometry α and delay time t_d and "magic" angle and neighborhood

So far we have limited the applications of our theory to the HHG signal for parallel geometry of the pump and probe polarizations. We now consider the more general case when probe polarization is rotated by a given angle α. Figure 12 shows our computational results of the HHG signals as a function of t_d, at various α, for N_2 (left panel) and for O_2 (right panel). We note that the signal for $\alpha=90°$ changes its phase by π with respect to the signal for $\alpha=0°$, a phenomenon that is also observed recently [12,27]. In contrast, the signal for $\alpha=45°$ is seen to remain rather flat with change of α.

To see the essential α dependence of the HHG signal of N_2, we consider the leading term of Eq. (113), which is given by

$$S^{(n)}(t_d;\alpha) = c_{00}^{(n)} + c_{01}^{(n)}\left[\frac{1}{2}\sin^2\alpha + \frac{1}{2}(3\cos^2\alpha - 1) \times \langle\langle\cos^2\theta\rangle\rangle(t_d)\right] + \cdots . \quad (130)$$

Thus, for the parallel polarizations we have $S^{(n)}(t_d;0°) \approx c_{00}^{(n)} + c_{01}^{(n)}\,\langle\langle\cos^2\theta\rangle\rangle\,(t_d)$ and for the perpendicular polarizations, $S^{(n)}(t_d;90°) \approx c_{00}^{(n)} + \frac{c_{01}^{(n)}}{2}\,[1 - \langle\langle\cos^2\theta\rangle\rangle(t_d)]$, which are clearly of opposite phase as a function of t_d. These expressions also show that the modulation depth for $\alpha=90°$ is smaller than the one for $\alpha=0°$, a fact that could not be accounted for by a planar model (e.g., [12]). Equation (130) also implies that the extrema of the signal would occur for $\sin\alpha\cos\alpha=0$, which predicts that the maximum would occur at $\alpha=0°$ and the minimum at $\alpha=90°$; this has been confirmed experimentally [12,26]. Equation (130) also predicts that there is a "magic" angle α_c given by $(3\cos^2\alpha_c - 1)=0$, i.e., $\alpha_c = \arctan\sqrt{2} \approx 55°$, where the time-dependent signals become the *same* for all delay t_d times. This geometry, therefore, can be used to generate a steady-state HHG signal from N_2. The magic angle at $\approx 55°$ in fact is a generic signature for the σ_g symmetry of the active molecular orbitals. Its presence in the data therefore can be helpful to identify the symmetry of the molecular orbital involved.

For O_2, the leading term of the HHG signal [Eq. (114)] reads

$$S^{(n)}(t_d;\alpha) = \frac{c_{11}^{(n)}}{64}\langle[(-35\cos^4\alpha + 30\cos^2\alpha - 3) \times\langle\cos^4\theta\rangle(t_d) + (30\cos^4\alpha - 24\cos^2\alpha + 2) \times\langle\cos^2\theta\rangle + (-3\sin^4\alpha + 4\sin^2\alpha)]^2\rangle + \cdots . \quad (131)$$

Thus, for the parallel polarizations we have $S^{(n)}(t_d;0°) \approx c_{11}^{(n)}\langle(-\langle\cos^4\theta\rangle + \langle\cos^2\theta\rangle)^2\rangle = c_{11}^{(n)}\langle\langle\sin^2\theta\cos^2\theta\rangle^2\rangle$ and for the perpendicular polarizations, $S(t_d;90°) \approx \frac{c_{11}^{(n)}}{64}\langle(-3\langle\cos^4\theta\rangle + 2\langle\cos^2\theta\rangle + 1)^2\rangle$. It is clear that the sign of $\langle\cos^4\theta\rangle$ does not change and hence the phase of the eighth revival also remains constant, as has been observed experimentally [12,27]. The above formula can be reexpressed as $S(t_d;90°) \approx c_{11}^{(n)}\ \langle(\frac{3}{8}\langle\sin^2\theta\cos^2\theta\rangle - \frac{1}{8}\langle\cos^2\theta\rangle + \frac{1}{8})^2\rangle$, which clearly shows that the modulation depth for $\alpha=90°$ is *smaller* than one for $\alpha=0°$, a result that cannot be obtained within a planar model (e.g., [12]).

Before concluding this section, it is also worthwhile to point out that the α dependence of the HHG signals for the more complex triatomic molecule CO_2, and the organic molecule acetylene, HC≡CH, because of the π symmetry of their active orbitals, as predicted (even without detailed calculations) by the general structure of the HHG signal, given by Eq. (103), will exhibit a "crossover" neighborhood near $\alpha \approx 55°$; this is indeed the case, as has been recently observed experimentally [62]. Clearly, the presence of the "magic" angle and the crossover neighborhood provide a signature of the symmetry of the active molecular orbital, which can be useful for the "inverse" problem of molecular imaging, as suggested in [20].

VII. ON SOME PROBLEMS OF GENERAL INTEREST RELATED TO PUMP-PROBE SIGNALS FOR HHG

Before concluding this paper, we report on the results of our investigations of a number of problems of general inter-

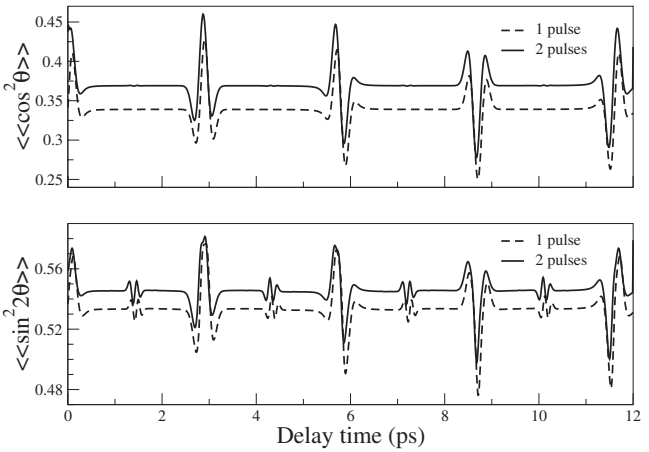

FIG. 13. Up shift of the alignment signal vs delay time: $\langle\langle\cos^2\theta\rangle\rangle$ for N_2 (upper panel) and $\langle\langle\sin^2 2\theta\rangle\rangle$ for O_2 (lower panel) at 300 K; $I_{\text{pump}}=0.8\times10^{14}$ W/cm^2 and $I_{\text{probe}}=1.7\times10^{14}$ W/cm^2 with FWHM 40 fs.

est in the present context of pump-probe experiments.

A. Effect of probe pulse on the alignment

In pump-probe experiments, it is generally assumed that the dynamical alignment of the molecular axis is governed by the ultrashort pump pulse, while the ultrashort probe pulse, which leads to the HHG signal, does not affect the alignment. To check the validity or otherwise of this assumption, we directly compare here the dynamic alignment moment, $A(t_d;\alpha=0)$, calculated as usual assuming when only the pump pulse and when both the pump and the delayed probe pulse couple to the molecular polarizability (for the case N_2). In the latter case, the total field consists of the superposition of the two pulses with a displacement Δt between them,

$$\boldsymbol{F}(t) = \boldsymbol{F}_1\cos(\omega_1 t) + \boldsymbol{F}_2\cos[\omega_2(t-\Delta t)] = \varepsilon_{10}\sqrt{g_1(t)}\cos(\omega_1 t) + \varepsilon_{20}\sqrt{g_2(t-\Delta t)}\cos[\omega_2(t-\Delta t)] \tag{132}$$

and

$$\langle F^2(t)\rangle = \frac{1}{2}\varepsilon_{10}^2 g_1(t) + \frac{1}{2}\varepsilon_{20}^2 g_2(t-\Delta t) + 2\varepsilon_{10}\varepsilon_{20} g_1(t) g_2(t-\Delta t) \times \langle[\cos(\omega_1 t)]\{\cos[\omega_2(t-\Delta t)]\}\rangle. \tag{133}$$

In the above, the indices 1 and 2 stand for pump and probe pulse, respectively. Suppose the data are recorded after the probe pulse dies out, then the observing time is $t=\Delta t+\tau$, where τ is the duration of the probe pulse.

In Fig. 13, we plot the alignment moment $\langle\langle\cos^2\theta\rangle\rangle(\Delta t+\tau)$ and $\langle\langle\sin^2 2\theta\rangle\rangle(\Delta t+\tau)$ for O_2 as a function of the delay Δt for a fixed $\tau=40$ fs, as shown by the solid curve. The result is compared with that obtained for the pump pulse alone (dashed curve) that is recorded at the same time. The comparison clearly shows that the probe pulse changes the dynamic alignment $\langle\langle\cos^2\theta\rangle\rangle(t_d)$ in that the signal is shifted upward by the presence of the probe pulse due to the enhanced effective intensity of the field. This relative up shift, however, does not change the general characteristics of the dynamical signals observed.

B. Effect of initial temperature

We assume that the rotational eigenstates $|J_0M_0\rangle$ of the molecule are occupied thermally before the interaction with the pump pulse. Unlike an upward transition $(J_0,M_0)\rightarrow(J_0',M_0)$ (in a linearly polarized field) to the states with an arbitrarily high J_0', the downward transition toward $J_0'\geqslant M_0$ would be more restricted, because of the conserved value of M_0. As a result, a wave-packet state created by the pump pulse would consist of eigenstates with higher occupation of $J_0'\geqslant M_0$ states, implying that the vector of rotational angular momentum would tend more to lie in a plane perpendicular to the pump polarization direction. Since the rotational angular momentum itself is perpendicular to the internuclear axis of a linear molecule, the above condition, $J_0'\geqslant M_0$, means also that the molecular axis would tend to align in the direction of the laser polarization. This is the physical reason why the alignment angle of the molecular axis with respect to the polarization direction after the laser interaction is generally smaller after the interaction than before it, i.e., the degree of alignment increases on interaction with the pump pulse. Since at a lower initial temperature the lower M_0 states, rather than the higher, are relatively more occupied initially, the "degree of alignment" $A\equiv\langle\langle\cos^2\theta\rangle\rangle$ would tend to be relatively higher, allowing the molecules to be more effectively aligned at a lower initial temperature (see Fig. 4 and 14).

C. Mean energy of the molecule after the pump pulse

It is interesting also to examine the way the mean energy of the molecule changes with increasing intensity of the pump pulse. Figure 15 shows the calculated mean energy $\langle E\rangle_{J_0M_0}(t)$ at a time t, before and after the arrival of the peak of the pump pulse (of length t_p). As expected, the figure shows that increasing the peak pulse intensity increases the mean energy of the molecule or the "effective temperature" $T_{\text{eff}}\equiv\langle E\rangle_{J_0M_0}(t>t_p)/k_B$, where k_B is the Boltzmann constant. However, it should be remembered that after the pulse interaction, the molecular system is not in a state of thermal equilibrium, rather it is in a state of dynamical equilibrium (or steady state) that cannot be characterized thermodynamically.

To estimate an effective "temperature" of the rotational wave-packet states $|\Phi_{J_0M_0}(t)\rangle$ in the steady-state regime after the interaction with the pump pulse, we note (a) that the rotational wave-packet states $|\Phi_{J_0M_0}(t)\rangle$ form a linearly independent complete set of states, like the set of rotational eigenstates $|J_0M_0\rangle$ from which they evolve, (b) that the individual rotational wave-packet states evolve in *one-to-one* correspondence with the initially occupied rotational eigenstates $|J_0M_0\rangle$, and (c) that the mean energy of each of the rotational wave-packet states reaches a steady state in energy from $\langle E\rangle_{J_0M_0}(t<-t_p/2)\rightarrow E_{J_0M_0}+\langle E\rangle_{J_0M_0}(t>t_p/2)$. If the above change in the mean energy is *independent* of the indi-

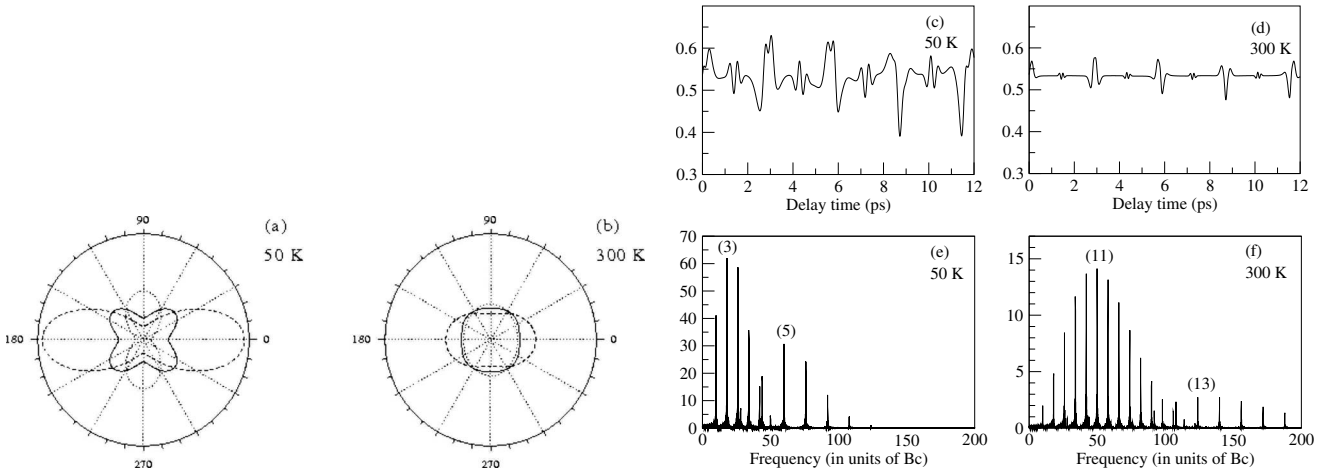

FIG. 14. Influence of the initial temperature, 50° or 300°, on the molecular axis distribution (panel a-b), on the leading dynamic moment $\langle\langle \sin^2 2\theta \rangle\rangle$ (t_d) (panel c-d), and the Fourier spectrum (panel e-f) of the latter, for the case of O_2. The molecular axis distribution (panel a-b) is given at three values of the delay t_d, i.e., at the "top" alignment t_d=5.649 ps (dashed line), at the "average" alignment t_d=5.812 ps (solid line), and at the "antitop" alignment t_d=5.975 ps (dotted line); the radii are in the same scale. $I=0.5\times10^{14}$ W/cm^2 and FWHM=40 fs.

vidual wave-packet states (indices $\{J_0M_0\}$), then one may ascribe the energy change to an effective "temperature" change, $\Delta T_{\rm eff}$, given by

$$\Delta T_{\rm eff} = \frac{\langle \Delta E \rangle (t > t_p/2)}{k_B}. \tag{134}$$

We may note from the results shown in Fig. 15 that the said change in the mean energy in the steady-state regime is indeed essentially independent of the states of the system. Thus, the effective "temperature" of the system, at the end of the interaction with the pump pulse, becomes

$$T_{\rm eff} = T_0 + \Delta T_{\rm eff}. \tag{135}$$

Note that $T_{\rm eff}$ is in general greater than the initial gas (jet) temperature, T_0, and it tends to increase with the increase of the pump intensity.

D. Comparison with some other nonequivalent definitions of the HHG signal

In this subsection, we briefly discuss two alternative definitions of HHG signals that have been employed earlier, and compare them with the definition of the HHG signal of the present theory (and experimental observations). As discussed in detail in the theory section, the present theory uses the quantum transition amplitudes for the coherent harmonic emission from and back to the linearly independent reference wave-packet states $|\chi_i(t)\rangle$, $i \equiv \{e, J_0M_0\}$ (consisting of the product of the ground electronic and the coherent rotational wave-packet states) to define the independent harmonic emission probabilities corresponding to the initial occupation of the rotational states. And in accordance with the quantum statistical theory, it averages the independent *probabilities* to define the observable HHG signal [cf., e.g., Eq. (62)],

$$S^{(n)}(t_d) = \mathcal{C} \sum_{J_0M_0} \rho(J_0) |\langle \Phi_{J_0M_0}(t_d,\theta)| \times T_e^{(n)}(\theta) |\Phi_{J_0M_0}(t_d,\theta)\rangle|^2. \tag{136}$$

It is worth noting that the quantum amplitude calculation in the present theory corresponds to the "adiabatic nuclei" approximation [60,61], in which the matrix elements with respect to the rotational wave-packet states are evaluated at the level of the adiabatic amplitude-operator, $T^{(n)}(\theta)$, and *not* at the level of the adiabatic probability operator, $|T^{(n)}(\theta)|^2$, that occurs in the more drastic "frozen nuclei" approximation. Also, in the present theory, as in the laboratory, the operational angle is the relative polarization angle α, and *not* the angle between the polarization direction and the molecular axis, θ. In fact, the angle θ is a rotational coordinate that, as required for a quantum formulation, is *integrated over* to obtain the quantum transition amplitudes (or the expectation values of Hermitian operators).

In the present notation, the two other definitions of the HHG signal that have been used earlier (to be referred to

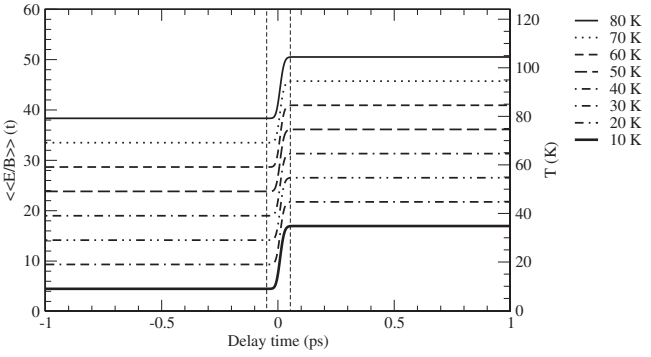

FIG. 15. Mean energy of O_2 before and after interaction with the laser pulse, for different initial temperatures. The vertical dashed lines indicate the extent of the pulse duration; $I=0.5\times10^{14}$ W/cm^2 and FWHM=40 fs.

below as A and B) are (i) definition A [cf. Eq. (22) of [25] and Eq. (6) of [63]],

$$S_A^{(n)}(t_d) = \mathcal{C}\left| \sum_{J_0 M_0} \rho(J_0) \langle \Phi_{J_0 M_0}(t_d,\theta)| \times T_e^{(n)}(\theta) |\Phi_{J_0 M_0}(t_d,\theta)\rangle \right|^2, \tag{137}$$

and (ii) definition B [cf. Eq. (12) of [24] and Eq. (4) of [64]],

$$S_B^{(n)}(t_d) = \mathcal{C} \sum_{J_0 M_0} \rho(J_0) \left| \langle \Phi_{J_0 M_0}(t_d,\theta)| \times |T_e^{(n)}(\theta)|^2 |\Phi_{J_0 M_0}(t_d,\theta)\rangle \right|. \tag{138}$$

Clearly the HHG signals according to models A and B differ from each other, and they differ from the present definition, Eq. (136) above.

We note that model A, Eq. (137), defines the statistically averaged signal by weighting the individual amplitudes first, and then taking the absolute square of the weighted sum. This procedure runs counter to the quantum statistical theoretical method of averaging the probabilities, *not* amplitudes, and/or the expectation values of Hermitian observables themselves, and not their Fourier transforms (that are proportional to the emission amplitudes). Furthermore, the definition of model A [Eq. (137)] causes the signal to depend on the mixed products of the statistical weights, which are in principle *independent*.

The signal defined by model B, Eq. (138), is seen to depend on the weighted sum of the diagonal matrix elements (between the rotational wave-packet states) of the "probability operator" $|T^{(n)}(\theta)|^2$—this, of course, is not equal to the weighted sum of the absolute squares of the diagonal matrix elements of the transition operator $T^{(n)}(\theta)$. In model B, the above circumstance is a consequence of the more drastic "frozen nuclei" approximation and an effective inclusion of *all* transitions, those between the same wave-packet states ("elastic-like") *as well as* those between the different wave-packet states ("inelastic-like"). However, unlike in model A [Eq. (137)], in model B [Eq. (138)] the weighted statistical sum is taken in accordance with the quantum statistical theory, at the level of the probabilities.

In Fig. 16, we show the Fourier spectrum of the dynamic signal (α=0) of the 19th harmonic, for the case of O_2, from the three test calculations, using (i) Eq. (136), the present theory (top panel); (ii) Eq. (137), model A (middle panel); and (iii) Eq. (138), model B (bottom panel), keeping everything else the same. The field parameters are as follows: pump $I=0.5\times10^{14}$ W/cm^2, probe $I=1.2\times10^{14}$ W/cm^2, pulse durations 40 fs, wavelengths 800 nm, and temperature 200 K.

We point out that the calculated spectrum from the present theory (upper panel) well reproduces the corresponding experimental data (cf. [[19], Fig. 2)—thus, for example, it reproduces all the spectral series observed experimentally for N_2 and O_2 as well as the ratio of the strengths of the major series observed. Model A also shows these series, however the ratios of the strengths of the series are not supported by the data. In the case of model B, on the other hand, the series V ($\boldsymbol{8},\boldsymbol{16},\boldsymbol{24},\ldots$)*Bc* is simply missing, and the relative strength of the major series is also not well supported by the data. It may be noted that the present comparison clearly illustrates the ability of the experimental data, at the level of the discrete Fourier spectrum, to better distinguish between the various theoretical models than may be practicable in the time domain.

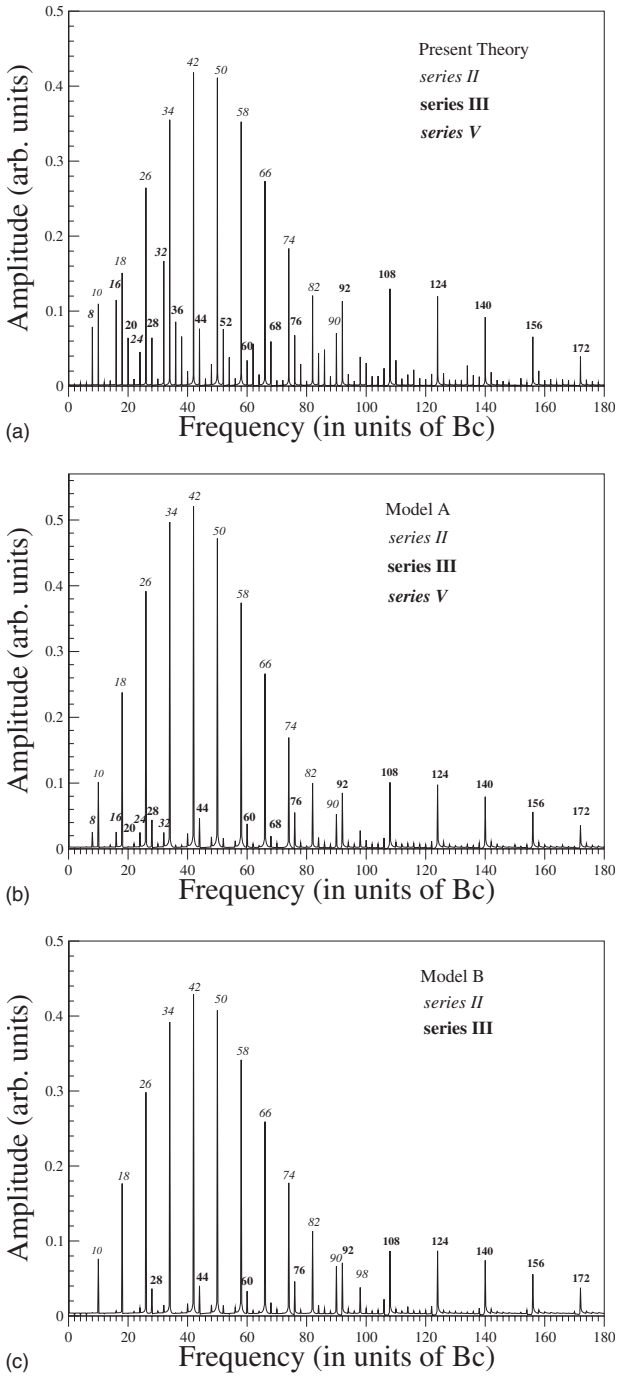

FIG. 16. Theoretical Fourier spectrum of the dynamic 19th harmonic signal for O_2; pump intensity $I=0.5\times10^{14}$ W/cm^2, probe intensity $I=1.2\times10^{14}$ W/cm^2, duration 40 fs, wavelength 800 nm, and temperature 200 K. The calculations are done using the present theory, Eq. (136) (upper panel), model A, Eq. (137) (middle panel), and model B, Eq. (138) (lower panel). For comparison to the experimental spectrum, please refer to [13,19].

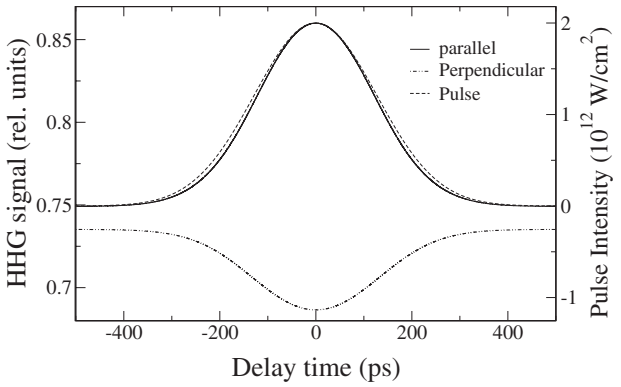

FIG. 17. Calculated 9th HHG spectrum of N_2 for various pump-probe polarizations angle $\alpha=0°$ and 90°; pump intensity $I=2\times10^{12}$ W/cm^2, duration 300 ps; probe intensity $I=5\times10^{14}$ W/cm^2, duration 70 fs, and wavelength 798 nm; Boltzmann temperature is 25 K.

E. Adiabatic alignment

Finally, we apply the present dynamic theory also to the adiabatic case, in which we choose a long (300 ps) pump pulse and a short (70 fs) probe pulse, as in an adiabatic alignment experiment [65] used earlier. The results of our calculations for N_2, using Eqs. (113) for both $\alpha=0°$ (solid curve) and $\alpha=90°$ (dash-dot curve), are shown in Fig. 17. For the sake of comparison, we also show the intensity profile (dashed curve) of the pump pulse (right scale). As can be seen immediately from the figure, in the parallel case, the HHG signal closely follows the evolution of the long pump pulse itself (which might be expected for an adiabatic process) and the maximum of the signal occurs at the maximum of pulse, for $\alpha=0°$. On the other hand, a minimum is predicted for the signal at the maximum intensity, in the perpendicular case, for $\alpha=90°$. These characteristics of the adiabatic signals for N_2 are consistent with the experimental observations made some time ago [65–67].

VIII. CONCLUSIONS

To conclude, we have presented an *ab initio* intense-field *S*-matrix theory of dynamic alignment of linear molecules and the characteristic HHG signals from them as detected in intense-field femtosecond pump-probe experiments. Useful analytical expressions for the molecular alignment and the HHG signal as a function of both the delay time t_d and the relative polarization angle α between the pump and probe pulse are derived. We give the general HHG signal for linear molecules, Eq. (103), the signal for N_2 (and generically, active σ_g orbital symmetry), Eq. (113), and its leading term, Eq. (130), as well as the signal for O_2 (and generically, active π_g orbital symmetry), Eq. (114), and its leading term, Eq. (131). They are used next to make a detailed analysis of the molecular alignment and the HHG experiments from coherently rotating N_2 and O_2 molecules. Results are obtained both in the time domain *and* in the frequency domain. The results show a remarkable agreement with all the salient characteristics of the experimental observations in N_2 and O_2. Additional predictions about the existence of critical relative polarization angles, α_c, and their relation to the symmetry of the active molecular orbitals and the form of the dynamic signals are made. At a "magic" angle, $\alpha_c\approx55°$, the dynamic HHG signals for all delay times t_d are predicted to approach each other closely for a σ_g orbital symmetry, or exhibit a "crossing neighborhood" in its vicinity, for the π_g orbital symmetry; specifically it is shown to produce a steady emission of high-order harmonic radiation, as well as a reversal of the phase of the dynamic signal, at the magic angle. Further, a number of theoretical questions and experimental effects of general interest, in connection with the interpretation of the pump-probe HHG signals, are investigated. Finally, it is shown that the case of "adiabatic-alignment," and the resulting HHG signal, can be analyzed and understood equally well within the present dynamical theory, using simply a long duration of the pump pulse.

[1] J. H. Posthumus, Rep. Prog. Phys. **67**, 623 (2004).
[2] A. Becker and F. H. M. Faisal, J. Phys. B **38**, R1 (2005).
[3] T. Seideman, Phys. Rev. Lett. **83**, 4971 (1999).
[4] J. Ortigoso, M. Rodriguez, M. Gupta, and B. Friedrich, J. Chem. Phys. **110**, 3870 (1999).
[5] L. Cai, J. Marango, and B. Friedrich, Phys. Rev. Lett. **86**, 775 (2001).
[6] H. Stapelfeldt and T. Seideman, Rev. Mod. Phys. **75**, 543 (2003).
[7] I. V. Litvinyuk, K. F. Lee, P. W. Dooley, D. M. Rayner, D. M. Villeneuve, and P. B. Corkum, Phys. Rev. Lett. **90**, 233003 (2003).
[8] P. W. Dooley, I. V. Litvinyuk, K. F. Lee, D. M. Rayner, M. Spanner, D. M. Villeneuve, and P. B. Corkum, Phys. Rev. A **68**, 023406 (2003).
[9] M. Kaku, K. Masuda, and K. Miyazaki, Jpn. J. Appl. Phys., Part 1 **43**, L591 (2004).
[10] D. Zeidler, J. Levesque, J. Itatani, K. Lee, P. W. Dooley, I. Litvinyuk, D. M. Villeneuve, and P. B. Corkum, in *Ultrafast Optics IV*, edited by F. Krauz *et al.* (Springer, New York, 2004), p. 247.
[11] J. Itatani, D. Zeidler, J. Levesque, M. Spanner, D. M. Villeneuve, and P. B. Corkum, Phys. Rev. Lett. **94**, 123902 (2005).
[12] T. Kanai, S. Minemoto, and H. Sakai, Nature **435**, 470 (2005).
[13] K. Miyazaki, M. Kaku, G. Miyaji, A. Abdurrouf, and F. H. M. Faisal, Phys. Rev. Lett. **95**, 243903 (2005).
[14] J. Itatani, J. Levesque, D. Zeidler, H. Niikura, H. Pepin, J. C. Kieffer, P. B. Corkum, and D. M. Villeneuve, Nature **432**, 867 (2004).
[15] J. Levesque, J. Itatani, D. Zeidler, H. Pepin, J. C. Kieffer, P. B. Corkum, and D. M. Villeneuve, J. Mod. Opt. **53**, 185 (2006).
[16] S. Patchkovskii, Z. Zhao, T. Brabec, and D. M. Villeneuve, Phys. Rev. Lett. **97**, 123003 (2006).
[17] S. Baker, J. S. Robinson, C. A. Haworth, H. Teng, R. A. Smith, C. C. Chirila, M. Lein, J. W. G. Tisch, and J. P. Marangos, Science **312**, 424 (2006).
[18] N. L. Wagner, A. Wuest, I. P. Christov, T. Popmintchev, X. Zhao, M. M. Murname, and H. C. Kapteyn, Proc. Natl. Acad.

Sci. U.S.A. **103**, 13279 (2006).
[19] F. H. M. Faisal, A. Abdurrouf, K. Miyazaki, and G. Miyaji, Phys. Rev. Lett. **98**, 143001 (2007).
[20] F. H. M. Faisal, and A. Abdurrouf, Phys. Rev. Lett. **100**, 123005 (2008).
[21] F. Rosca-Pruna and M. J. J. Vrakking, J. Chem. Phys. **116**, 6579 (2002).
[22] G. Herzberg, *Molecular Spectra and Molecular Structure, I.* (Van Nostrand Reinhold, New York, 1950), Chap. III.
[23] X. X. Zhou, X. M. Tong, Z. X. Zhao, and C. D. Lin, Phys. Rev. A **71**, 061801(R) (2005).
[24] X. X. Zhou, X. M. Tong, Z. X. Zhao, and C. D. Lin, Phys. Rev. A **72**, 033412 (2005).
[25] C. B. Madsen and L. B. Madsen, Phys. Rev. A **74**, 023403 (2006).
[26] M. Kaku, R. Morichi, G. Miyaji, and K. Miyazaki, IEEE on Quantum Electronics Conference 2005, paper QWG4–3, p. 1036.
[27] K. Yoshii, G. Miyaji, K. Miyazaki, A. Abdurruf, and F. H. M. Faisal, IEEE on CLEO-Pacific Rim 2007 (2007), p. 660.
[28] We may assume as usual that the field envelopes, $f(t)$, are slowly varying compared, e.g., to the period associated with a harmonic frequency $\Omega=n\omega$, or, $\frac{\partial f(t)}{\partial t}/f(t)\ll\Omega$.
[29] R. P. Feynman, *Quantum Electrodynamics* (Benjamin Inc., New York, 1962).
[30] J. J. Sakurai, *Modern Quantum Mechanics* (Addison-Wesley, New York, 1994).
[31] L. V. Keldysh, Zh. Eksp. Teor. Fiz. **47**, 1945 (1964) [Sov. Phys. JETP **20**, 1307 (1964)].
[32] F. H. M. Faisal, J. Phys. B **6**, 89 (1973).
[33] H. R. Reiss, Phys. Rev. A **22**, 1786 (1980).
[34] J. D. Jackson, *Classical Electrodynamics* (Wiley, New York, 1962).
[35] W. H. Press, B. P. Flannery, S. A. Teukolsky, and W. T. Vetterling, *Numerical Recipes: The Art of Scientific Computing* (Cambridge University Press, Cambridge, 1986).
[36] P. Salières, B. Carré, L. Le Déroff, F. Grasbon, G. G. Paulus, H. Walther, R. Kopold, W. Becker, D. B. Milosevic, A. Sanpera, and M. Lewenstein, Science **292**, 902 (2001).
[37] We may note that the above holds strictly for an ideal medium with a constant velocity of propagation. In dispersive media, the frequency and the wave numbers are related by the frequency-dependent velocity of propagation $v=c/n(\Omega)$, where n is the frequency-dependent refractive index of the medium. This necessitates a much more detailed analysis of the phase-matching condition, which has been carried out (see, e.g., [36]) by solving numerically the coupled Maxwell's equations for the propagating fields, in specific cases. The results indicate, rather generally, an effective phase matching for the higher harmonics. In the presence of ionization, the medium becomes also dissipative. In a weakly ionized medium, the effect may be taken into account by including a decay factor $e^{-(1/2)\gamma_i(t+t')}$ that is to be multiplied with the expression of the integrand of the HHG amplitude (or of the dipole expectation value), where γ_i is the total rate of ionization of the reference bound state $i\equiv|\chi_i(t)\rangle$.
[38] X. F. Li, A. L'Hullier, M. Ferray, L. A. Lompre, and G. Mainfray, Phys. Rev. A **39**, 5751 (1989).
[39] A. McPherson, G. Gibson, H. Jara, U. Johann, T. S. Luk, I. A. McIntyre, K. Boyer, and C. K. Rodes, J. Opt. Soc. Am. B **4**, 595 (1987).
[40] F. Ehlotzky, Phys. Rep. **345**, 175 (2001).
[41] T. Seideman, J. Chem. Phys. **115**, 5965 (2001).
[42] M. Lewenstein, Ph. Balcou, M. Yu. Ivanov, A. L'Huillier, and P. B. Corkum, Phys. Rev. A **49**, 2117 (1994).
[43] F. E. Harris and H. H. Michels, J. Chem. Phys. **43**, S165 (1965).
[44] F. H. M. Faisal, J. Phys. B **3**, 636 (1970).
[45] D. A. Varshalovich, A. M. Moskalev, and V. K. Khersonskii, *Quantum Theory of Angular Momentum* (World Scientific, Singapore, 1988).
[46] R. N. Zare, *Angular Momentum: Understanding Spatial Aspects in Chemistry and Physics* (Wiley, New York, 1988).
[47] I. S. Gradshteyn and I. M. Rhysik, *Table of Integral, Series, and Product* (Academic, New York, 1965).
[48] X. M. Tong, Z. X. Zhao, and C. D. Lin, Phys. Rev. A **66**, 033402 (2002).
[49] T. K. Kjeldsen and L. B. Madsen, Phys. Rev. A **71**, 023411 (2005).
[50] W. L. Jorgensen and L. Salem, *The Organic Chemist's Book of Orbital* (Academic, New York, 1973).
[51] A. M. James and M. P. Lord, *MacMillan's Chemical Physical Data* (MacMillan, London, 1992).
[52] J. O. Hirschfelder, C. F. Curtis, and R. B. Bird, *Molecular Theory of Gases and Liquids* (Wiley, New York, 1954).
[53] S. Ramakrishna and T. Seideman, Phys. Rev. Lett. **99**, 113901 (2007).
[54] S. Ramakrishna and T. Seideman, Phys. Rev. A **77**, 053411 (2008).
[55] F. Rosca-Pruna and M. J. J. Vrakking, J. Chem. Phys. **116**, 6567 (2002).
[56] I. Sh. Averbukh and N. F. Parelman, Phys. Lett. A **139**, 449 (1989).
[57] M. J. J. Vrakking, D. M. Villeneuve, and A. Stolow, Phys. Rev. A **54**, R37 (1996).
[58] R. Bluhm, V. A. Kostelecky, and J. A. Porter, Am. J. Phys. **64**, 944 (1996).
[59] S. Fleischer, I. Sh. Averbukh, and Y. Prior, Phys. Rev. A **74**, 041403(R) (2006).
[60] D. M. Chase, Phys. Rev. **104**, 838 (1956).
[61] F. H. M. Faisal and A. Temkin, Phys. Rev. Lett. **28**, 203 (1972).
[62] R. Torres, N. Kajumba, J. G. Underwood, J. S. Robinson, S. Baker, J. W. G. Tisch, R. de Nalda, W. A. Bryan, R. Velotta, C. Altucci, I. C. E. Turcu, and J. P. Marangos, Phys. Rev. Lett. **98**, 203007 (2007).
[63] C. B. Madsen, A. S. Mouritzen, T. K. Kjeldsen, and L. B. Madsen, Phys. Rev. A **76**, 035401 (2007).
[64] A. T. Le, X.-M. Tong, Phys. Rev. A **73**, 041402(R) (2006).
[65] R. Velotta, N. Hay, M. B. Mason, M. Castillejo, and J. P. Marangos, Phys. Rev. Lett. **87**, 183901 (2001).
[66] N. Hay, R. Velotta, M. Lein, R. de Nalda, E. Heesel, M. Castillejo, and J. P. Marangos, Phys. Rev. A **65**, 053805 (2002).
[67] N. Hay, M. Lein, R. Velotta, R. deNalda, E. Hessel, M. Castillejo, P. L. Knight, and J. P. Marangos, J. Mod. Opt. **50**, 561 (2003).